the pathogenesis of envenomation by the Japanese colubrid snake, Yamakagashi, *Rhabdophis tigrinus tigrinus*. The Snake, **22**, 11-19.

Sakai, A., Honma, M. and Sawai, Y. (1983): Studies on the pathogenesis of envenomation of the Japanese colubrid snake, Yamakagashi, *Rhabdophis tigrinus tigrinus* (Boie). The Snake, **15**, 7-13.

Sakai, A., Honma, M. and Sawai, Y. (1984): Study on the toxicity of venoms expressed from Duvernoy's gland of certain Asian colubrid snakes. The Snake, **16**, 16-20.

Takeya, H., Nishida, S., Miyata, T., Kawada, S., Saisaka, Y., Morita, T. and Iwanaga, S. (1992): Coagulation factor X activating enzyme from Russell's viper venom (RVV-X). J. Biol. Chem., **267**, 14109-14117.

Takeya, H., Miyata, T., Nishino, N., Omori-Satoh, T. and Iwanaga, S. (1993): Snake venom Hemorrhagic and Nonhemorrhagic metalloproteinases. In Methods in Enzymology, Vol.223 (Abelson,J.N. and Simon, M.L., eds.), pp. 365-379, Academic Press, San Diego.

Tu, A.T. (1991): In Handbook of Natural Toxins, Vol. 5 (Tu, A.T., ed.), pp.297-347, Mercel Dekker, New York.

Van Wart, E.D. and Birkedal-Hansen, H. (1990): The cysteine switch: A principle of regulation of metalloproteinase activity with potential applicability to the entire matrix metalloproteinase gene family. Proc. Natl. Acad. Sci., **87**, 5578-5582.

Available online at www.sciencedirect.com

ScienceDirect

ELSEVIER

Biochemical and Biophysical Research Communications 350 (2006) 1026–1031

BBRC

www.elsevier.com/locate/ybbrc

Isolation and identification of proangiotensin-12, a possible component of the renin–angiotensin system

Sayaka Nagata [a], Johji Kato [a,*], Kazuki Sasaki [b], Naoto Minamino [b], Tanenao Eto [a], Kazuo Kitamura [a]

[a] *Circulatory and Body Fluid Regulation, Faculty of Medicine, University of Miyazaki, 5200 Kihara, Kiyotake, Miyazaki 889-1692, Japan*
[b] *National Cardiovascular Center Research Institute, Fujishirodai, Suita, Osaka 565, Japan*

Received 20 September 2006
Available online 5 October 2006

Abstract

The renin–angiotensin (RA) system plays an important role in regulating blood pressure and fluid balance. In the search for bioactive peptides with an antibody binding to the N-terminal portion of angiotensin II (Ang II), we isolated a new angiotensinogen-derived peptide from the rat small intestine. Consisting of 12 amino acids, this peptide was termed proangiotensin-12 based on its possible role of an Ang II precursor. Proangiotensin-12 constricted aortic strips and, when infused intravenously, raised blood pressure in rats, while both the vasoconstrictor and pressor response to proangiotensin-12 were abolished by captopril and by CV-11974, an Ang II type I receptor blocker. Proangiotensin-12 is abundant in a wide range of organs and tissues including the small intestine, spleen, kidneys, and liver of rats. The identification of proangiotensin-12 suggests a processing cascade of the RA system, different from the cleavage of angiotensinogen to Ang I by renin.
© 2006 Published by Elsevier Inc.

Keywords: Proangiotensin-12; Renin–angiotensin system; Pressor peptide; Angiotensinogen; Processing

A number of mechanical or humoral mechanisms are involved in blood pressure and body fluid homeostasis in mammals. Among them, the renin–angiotensin (RA) system plays a pivotal role, regulating the vascular tone of resistant vessels and glomerular filtration or re-absorption of electrolytes in the kidneys. The protease enzyme renin secreted from kidneys cleaves specifically angiotensinogen circulating in the blood to produce angiotensin I (Ang I), a peptide consisting of 10 amino acid residues, which in the presence of angiotensin-converting enzyme (ACE), is in turn converted to Ang II, a potent pressor peptide mediating the major actions of the RA system as a circulating hormone [1,2]. On the other hand, recent research has revealed new aspects of the RA system. For example, the tissue RA system has been vigorously studied, and its activation is assumed to be regulated independently of the systemic RA system [3–5]. Another example is the identification of Ang II-derived peptides that are shorter than Ang II, such as Ang(1–7), Ang III, or Ang IV, having pharmacological properties different from those of Ang II [6–11]. Meanwhile, consisting of 10 amino acid residues, Ang I has been thought to be produced by renin directly from angiotensinogen, a protein of 452 amino acids for humans or 453 for rats [12,13], but there has been no report on the occurrence of angiotensinogen-derived peptides of amino acid sequences longer than Ang I. In the present study, on searching for peptides structurally related to Ang II, we purified an angiotensinogen-derived pressor peptide of 12 amino acids, which is thought to be one of the major components of the RA system.

Materials and methods

Reagents and animals. Ang I and Ang II were purchased from Peptide Institute Inc. (Osaka, Japan) and proangiotensin-12 was synthesized by Bex. Co., Ltd. (Tokyo, Japan). CV-11974 was kindly provided by Takeda

* Corresponding author. Fax: +81 985 85 6596.
E-mail address: jkjpn@med.miyazaki-u.ac.jp (J. Kato).

0006-291X/$ - see front matter © 2006 Published by Elsevier Inc.
doi:10.1016/j.bbrc.2006.09.146

Pharmaceutical Company Limited (Osaka, Japan). Wistar rats of 6–7 weeks of age were purchased from Charles River Laboratories (Kanagawa, Japan) and New Zealand white rabbits from Kyudo Co., Ltd. (Saga, Japan). The present study was performed in accordance with the Animal Welfare Act and with approval of the University of Miyazaki Institutional Animal Care and Use Committee (2004-100-2, 2004-101-2).

Detection of immunoreactive N-terminal Ang II. To prepare antiserum against the N-terminal of Ang II, synthesized Ang II-Cys was conjugated with *keyhole limpet* hemocyanin at room temperature over 2 h. After dialyses repeated four times in 50 mmol/L PBS, the conjugate solution was emulsified with an equal volume of Titer Max Gold (Sigma–Aldrich, Tokyo, Japan) and injected subcutaneously into New Zealand white rabbits every two weeks over three months. A specific radioimmunoassay (RIA) was prepared with the antiserum obtained from an immunized rabbit, as previously described [14,15]. This RIA cross-reacted with Ang I and Ang III at levels of 50% and 12.5%, respectively, without cross-reactions with Ang IV and Ang(1–7). To characterize the immunoreactive N-terminal Ang II in tissues, 1.0 g of sample from various rat tissues was immediately boiled for 10 min and acidified with acetic acid to a final concentration of 1.0 mol/L to inactivate proteases. Then the samples were homogenized and centrifuged for 20 min at 12,000 rpm, and the supernatant was applied to Sep-Pak C18 cartridges. After elution with 60% CH_3CN in 0.1% trifluoroacetic acid, the peptide extracts were subjected to reverse-phase high-performance liquid chromatography (RP-HPLC) with an ODS-120A column, and the immunoreactive N-terminal Ang II of each fraction was measured by the RIA.

Purification procedure. The peptide extract was obtained with the above-described method from 380 g of small intestine, a rat tissue showing the largest peak of immunoreactive N-terminal Ang II at a position clearly different from that of Ang I or Ang II in the RP-HPLC analysis. The sample was applied to a SP Sephadex C-25 column eluted with 2.0 mol/L pyridine, and subjected to gel filtration with Sephadex G-50 and an affinity column (Affi-Gel 10 Active Ester Agarose, Bio-Rad) which had been prepared with the anti-N-terminal Ang II antiserum. These purification steps were done while monitoring immunoreactive N-terminal Ang II with the RIA. The extract was further purified by three steps of HPLC with columns of ODS-120A, diphenyl, and Chemco sorb3-ODS-H. The amino acid sequence of the finally purified peptide was analyzed by a time-of-flight mass spectrometric method.

Mass spectrometry. To determine the amino acid sequence and molecular weight of the purified peptide, a tandem mass spectrometric analysis was performed with positive electrospray ionization using a QTof-2 quadrupole time of flight mass spectrometer (Micromass, UK). The sample was dissolved in a solution of water/methanol/acetic acid mixed at 49:49:2 by volume and nanosprayed from off-line MS emitters (Proxeon, Denmark) with a capillary voltage of 1.5 kV and a cone voltage of 30 V. The mass spectrum was acquired from m/z 200 to 2000. For tandem mass spectrometry, the triply charged ion with m/z 524.97 was subjected to collision-induced dissociation with argon gas in the 30 eV collision energy range. Data acquisition and processing were performed using MassLynx v4.0 (Micromass). The resultant tandem mass spectrum was subjected to a Mascot MS/MS ion search (Matrixscience, UK) and also interpreted by PepSeq (Micromass).

Radioimmunoassay for the C-terminal portion of proangiotensin-12. To specifically detect proangiotensin-12 in tissues and plasma, we developed a RIA, as previously described, with antiserum raised against the C-terminal portion of the peptide [14,15]. Synthetic proangiotensin-12 was conjugated with bovine thyroglobulin at room temperature for 15 min by the glutaraldehyde method. New Zealand white rabbits were immunized with the dialyzed conjugate, according to the procedure described above. After the immunization, specific antibody was purified from the antiserum using an affinity column (NHS-activated Sepharose 4 Fast Flow) with the C-terminal peptide of proangiotensin-12, Ile-His-Pro-Phe-His-Leu-Leu-Tyr. The proangiotensin-12 levels in tissues and plasma of male Wistar rats were determined by RIA with the purified antibody, following extraction with a Sep-Pak C18 cartridge, as described previously [14,15]. This RIA detected 1.6 and 3.1% of angiotensinogen(1–14) and angiotensinogen(1–17), respectively, but showed no cross-reactivity with Ang I, Ang II, Ang III, Ang IV, or Ang(1–7). The Ang I or Ang II levels in tissues and plasma were similarly determined by RIAs with anti-C-terminal of Ang I and Ang II antisera purchased from Miles and Cortex Biochem, Inc. (San Leandro, USA), respectively [16,17]. To characterize the immunoreactive C-terminal proangiotensin-12 in the extract of rat small intestines, a RP-HPLC analysis was done with an ODS-120A column as described above.

Pharmacological studies ex vivo and in vivo. We examined the effects of proangiotensin-12 on vascular tone with perfused aorta isolated from rats as reported previously [18]. The aortic rings were mounted under a passive tension of 1.0 g in organ baths containing Krebs–Henseleit solution oxidized with 95% O_2 and 5% CO_2 at 37 °C, and left for 60 min for equilibration. The viability of the aortic rings was confirmed by exposing the samples to 60 mmol/L KCl, 10^{-7} mol/L phenylephrine, and 10^{-6} mol/L acetylcholine. Contractions of the aortic samples were recorded before and after Ang I, Ang II, or proangiotensin-12 was added to the perfusion solution at the indicated concentration. The responses to these peptides were also tested in the presence of 10^{-7} mol/L captopril, an ACE inhibitor, or 10^{-8} mol/L CV-11974, an Ang II type 1 (AT1) receptor antagonist. Next, the effects of proangiotensin-12 on blood pressure were examined *in vivo* with rats fed a normal rat chow, as previously described [19]. Male Wistar rats weighing 220–260 g were anesthetized with an intraperitoneal injection of 50 mg/kg pentobarbital sodium. Synthetic proangiotensin-12 dissolved in 100 µl saline was injected into the jugular vein at the bolus-dose indicated, and blood pressure and heart rate were monitored before and after the injection by a carotid artery catheter connected to a pressure transducer with the Power Lab system (MLT0699 Disposable BP Transducer, AD Instruments, Australia). The responses to proangiotensin-12 were similarly tested 2 min after the intravenous injection of 0.03 mg/kg captopril or 0.3 mg/kg CV-11974.

Statistical analysis. Comparisons of all data were made with an analysis of variance (ANOVA) followed by Scheffe's test. Values are presented as means ± SE and statistical significance was set at $P < 0.05$.

Results

Purification of proangiotensin-12

As a first step in the isolation of Ang II-related peptides, we analyzed immunoreactive N-terminal Ang II in peptide samples extracted from various tissues of rats with RP-HPLC and a RIA. In those analyses, we found three clear peaks of immunoreactive N-terminal Ang II in rat tissues including the small intestine (Fig. 1): the earliest peak and the next peak corresponded to Ang II and Ang I, respectively. Interestingly, the largest peak emerged later

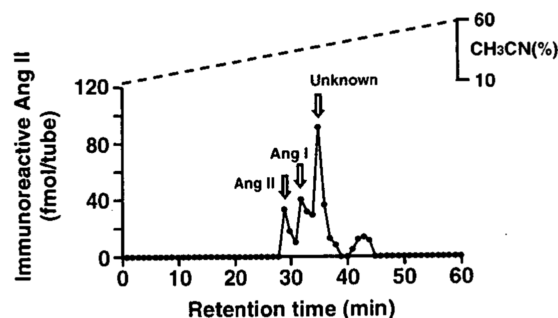

Fig. 1. Immunoreactive N-terminal Ang II in rat small intestine. An extract of the small intestine was subjected to RP-HPLC, where the immunoreactive N-terminal Ang II of each fraction was determined by specific radioimmunoassay, as described. An elution gradient of 10% to 60% CH_3CN was made in 0.1% trifluoroacetic acid over 60 min with a flow rate at 1 ml/min.

than Ang I in the small intestine, suggesting the presence of an unknown peptide similar in sequence to the N-terminal portion of Ang II. Therefore, we tried to purify this unknown peptide from 380 g of rat small intestine by several steps of ion-exchange, gel-filtration, and affinity chromatography, and RP-HPLC, as described in the Materials and methods section. Fig. 2A shows the final step of purification with RP-HPLC, where the unknown peptide was obtained as a single peak. The purified peptide sample was then subjected to the tandem mass spectrometry and found to consist of 12 amino acid residues (Fig. 2B). In comparison of the sequences of Ang I and the N-terminal portion of angiotensinogen, the unknown peptide was deduced to be a C-terminal extended form of Ang I (Fig. 3). We have termed this novel peptide proangiotensin-12, based upon the results of the tissue distribution and pharmacological experiments of the present study, suggesting a role for this peptide as a precursor of Ang II.

Measurement of tissue and plasma levels of proangiotensin-12

Next, we developed a radioimmunoassay specifically detecting the C-terminal portion of proangiotensin-12 to clarify the presence of this novel peptide in rat tissues including the small intestine. As shown in Table 1, proangiotensin-12 was abundantly detected in a variety of tissues, where its levels were higher than those of Ang I or Ang II, except for the lungs, adrenal glands, pancreas, and aorta. These tissue levels determined by the RIA specific to the C-terminal were found to be mostly identical to those estimated by an immunoreactive peak corresponding to proangiotensin-12 (Fig. 1) by RP-HPLC analyses with RIA detecting the N-terminal Ang II. In contrast to the tissue levels, the plasma concentration of proangiotensin-12 was lower than that of Ang I or

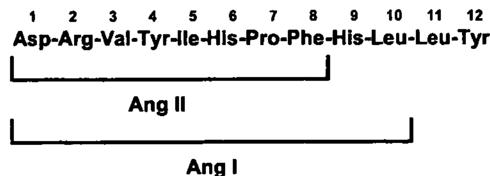

Fig. 3. Amino acid sequence of proangiotensin-12.

Table 1
Specific measurement of immunoreactive proangiotensin-12, Ang I, and Ang II levels in rat tissues and plasma

	Proangiotensin-12	Ang I	Ang II
Small intestine	663.1 ± 123.3	283.6 ± 43.0	254.9 ± 48.3
Spleen	419.1 ± 18.4	71.1 ± 4.0	302.0 ± 8.7
Kidneys	380.3 ± 27.0	365.2 ± 29.7	116.4 ± 6.9
Liver	252.0 ± 13.8	79.6 ± 2.6	87.9 ± 4.6
Stomach	241.7 ± 15.5	148.2 ± 23.0	81.5 ± 6.8
Lungs	227.8 ± 20.1	56.7 ± 5.7	236.2 ± 31.7
Adrenal glands	223.8 ± 8.2	121.4 ± 27.7	3049.2 ± 779.5
Heart	150.6 ± 11.3	84.9 ± 7.8	42.3 ± 7.3
Brain	147.4 ± 8.1	52.0 ± 2.7	29.6 ± 3.6
Pancreas	87.2 ± 13.8	37.8 ± 11.6	93.0 ± 17.6
Aorta	24.1 ± 7.5	39.6 ± 2.4	118.5 ± 6.6
Plasma	10.1 ± 2.7	382.5 ± 79.9	28.9 ± 8.8

The tissue or plasma levels of proangiotensin-12 were determined by a radioimmunoassay specifically detecting the C-terminal portion of the peptide as described in the Materials and methods section. The tissues are listed in order of immunoreactive proangiotensin-12 levels. The results are shown as means ± SE for eight rats examined (fmol/g tissue or fmol/ml plasma).

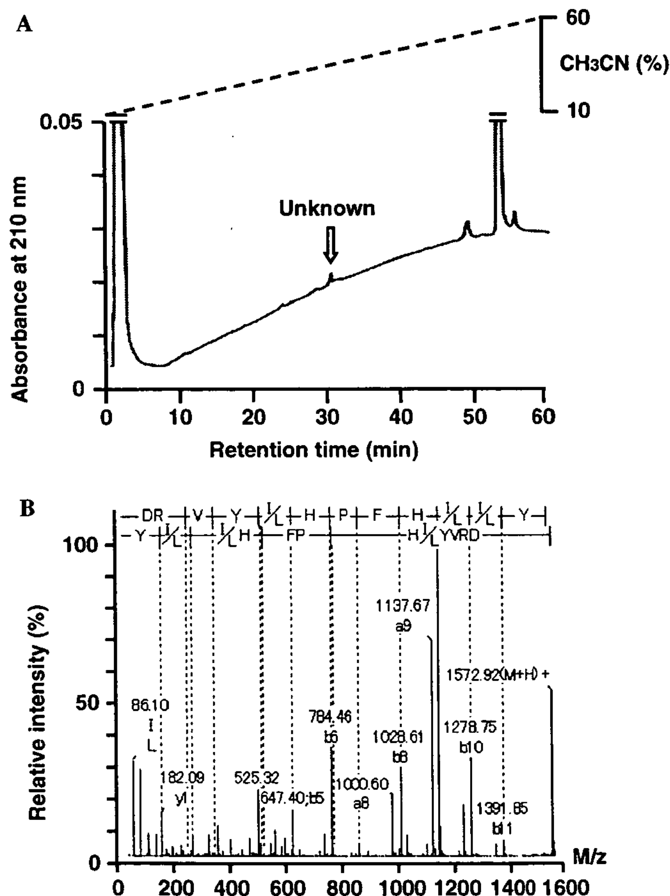

Fig. 2. Final purification by RP-HPLC (A) and tandem mass spectrometric analysis of the purified peptide (B).

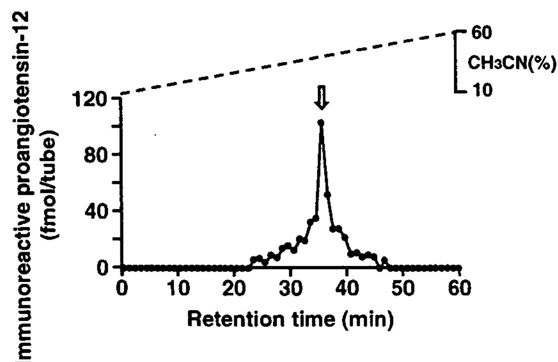

Fig. 4. Characterization of immunoreactive C-terminal proangiotensin-12 in rat small intestine by RP-HPLC and radioimmunoassay. RP-HPLC was conducted as described in the legend for Fig. 1. The arrow indicates the position of the full-length synthetic proangiotensin-12 peptide.

Ang II. The HPLC analysis revealed that immunoreactive proangiotensin-12 in the small intestine was eluted at the same position as the complete synthetic peptide (Fig. 4), further confirming the amino acid sequence and presence of proangiotensin-12.

Pharmacological studies ex vivo and in vivo

To study the biological actions of proangiotensin-12, we first looked at the effects on the vascular tonus of perfused rat aortic rings *ex vivo*. As shown in Fig. 5, proangiotensin-12 dose-dependently constricted the rat aorta as did Ang I or Ang II. Ang I and proangiotensin-12 had weaker vasoconstrictor effects than Ang II at concentrations of 3–30 nmol/L, but similar maximum contractions were obtained at 100 nmol/L of all three peptides. The constrictor action of proangiotensin-12 was mostly abolished in the presence of captopril, an ACE inhibitor, or CV-11974, an AT1 receptor blocker. Next, we examined the effects of proangiotensin-12 on blood pressure levels *in vivo* in anesthetized rats. A rise in arterial blood pressure was observed immediately after the intravenous injection of a bolus of proangiotensin-12 in rats, with a return to the basal level in 3–4 min (Fig. 6A). The pressor effects were dose-dependent and attenuated by pre-administration of captopril or CV-11974 (Figs. 6B and C), a result consistent with the *ex vivo* study.

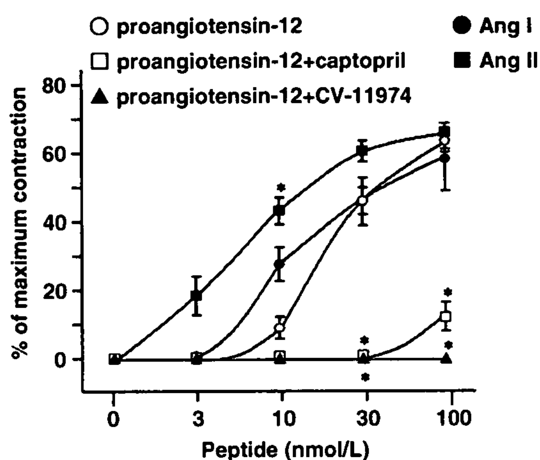

Fig. 5. Vasoconstrictor effects of Ang I, Ang II, and proangiotensin-12 on perfused rat aorta *ex vivo*. Captopril and CV-11974, an AT1 receptor antagonist, were used at 10^{-7} and 10^{-8} mol/L, respectively. The results are shown as means ± SE of % of maximum contraction induced by 60 mmol/L KCl for six to seven samples. $^*P < 0.05$ vs proangiotensin-12 alone.

Discussion

In this report, we describe the purification, sequence determination, tissue distribution, and vasoconstrictor properties of the novel angiotensinogen-derived peptide, Ang I-Leu-Tyr, which consists of 12 amino acid residues. We have termed this novel peptide proangiotensin-12, based upon the present results that suggest its role as a precursor of Ang II.

A concern may be raised over non-specific cleavage between Tyr-12 and Ser-13 of rat angiotensinogen, resulting in the occurrence of proangiotensin-12 as a non-specifically fragmented product during the extraction procedure; however, this possibility is unlikely based on the following reasons or findings. First, samples of rat small intestine were immediately boiled and acidified after resection in

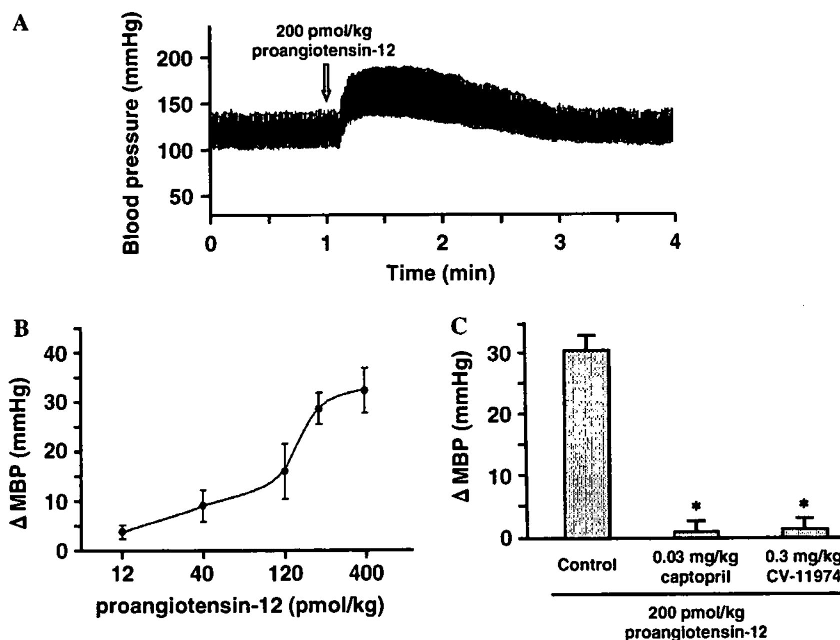

Fig. 6. (A) Representative blood pressure recording following the intravenous injection of a 200 pmol/kg bolus of proangiotensin-12 in anesthetized rats, (B) dose-dependent pressor effects, and (C) attenuation of the effects of proangiotensin-12 by captopril or CV-11974, an AT1 receptor blocker. ΔMBP indicates the maximum rise of mean blood pressure from the baseline. Either captopril or CV-11974 was intravenously injected at the indicated dose 2 min before the injection of proangiotensin-12. The results are shown as means ± SE for five rats examined. $^*P < 0.05$ vs proangiotensin-12 alone.

the extraction procedure. Non-specific cleavage of peptides can be avoided with this step which inactivates enzymes with proteolytic activity [20,21]. Second, the HPLC analysis of immunoreactive N-terminal Ang II (Fig. 1) showed three clear peaks, which correspond to Ang II, Ang I, and proangiotensin-12, without fragmentation of peptides. The specific radioimmunoassay (Table 1) also revealed that proangiotensin-12 is ubiquitously present in various organs and tissues, as are Ang I and Ang II. Last, the immunoreactive proangiotensin-12 in the small intestine was eluted at the position of the full-length peptide in the RP-HPLC analysis and radioimmunoassay detecting the C-terminal portion of proangiotensin-12 (Fig. 4). These findings are clearly indicative of the endogenous occurrence of proangiotensin-12.

A number of mechanisms, either mechanical or humoral, have been known to be involved in regulating blood pressure and body fluid balance in mammals. Among the humoral factors, the RA system plays a pivotal role: renin secreted mainly from kidneys cleaves angiotensinogen circulating in the blood to produce Ang I, which is then converted to Ang II exerting various effects particularly important for blood pressure and body fluid homeostasis. In the meantime, recent progress in research has revealed new aspects of the RA system. One example is identification of the Ang II-derived bioactive peptides with amino acid sequences shorter than Ang II such as Ang(1–7), Ang III or Ang IV [6–11]. Given this fact, it should be noted that proangiotensin-12 is a peptide longer than Ang I and such an angiotensinogen-derived peptide had not been identified. The second example is an active role of the tissue RA system probably independent of the systemic RA system [3–5]. In the present study, radioimmunoassay specifically detecting the C-terminal portion of proangiotensin-12 revealed ubiquitous presence of this novel peptide in various tissues and organs at the concentrations comparable with those of Ang I and Ang II, while the plasma concentration was lower than that of Ang I or Ang II. The relatively higher tissue levels suggest a significant role of proangiotensin-12 as a molecule of the tissue RA system.

In the present study, proangiotensin-12 exerted vasoconstrictor activity *ex vivo* on rat aortic rings, potency of which was similar to Ang I, while somehow weaker than Ang II at concentration of 3–30 nmol/L, showing the maximum contraction similar to Ang II. When injected intravenously in rats, proangiotensin-12 immediately raised blood pressure levels, and both the vasoconstrictor and pressor effects mostly disappeared following administration of captopril or CV-11974, an AT1 receptor blocker. These findings suggest prompt conversions of proangiotensin-12 to Ang I, and then Ang I to Ang II by ACE. Although the enzymes involved in the conversion to Ang I remain to be identified, the prompt cleavages of proangiotensin-12 to produce Ang II support the hypothesis of a significant role of proangiotensin-12 as an important molecule of the RA system.

Angiotensinogen is recognized to be produced and supplied to the blood mainly by the liver, though this precursor protein has been shown to be expressed widely in other tissues [22–25]. Consistent with this, according to our quantitative PCR, angiotensinogen mRNA was detected in various rat organs and tissues including the small intestine with the highest level in liver (data not shown). Because renin is an exclusively specific enzyme which cleaves angiotensinogen directly to produce Ang I, it is unlikely that renin is involved in the production of proangiotensin-12 [1,2]. An important question related to this is where the cleavage of angiotensinogen to proangiotensin-12 occurs: in tissues or in plasma. Clarifying the processing cascade of angiotensinogen would therefore provide us with information not only on the production of proangiotensin-12 but also on the mechanism activating the RA system and the role of proangiotensin-12 in blood pressure and body fluid homeostasis. Indeed, we are currently working on characterization and purification of enzymes that produce or cleave proangiotensin-12. Additionally, it should be clarified whether or not Ang I precursor peptides similar to proangiotensin-12 are present in other species including humans. Thus, the identification of proangiotensin-12 warrants future research on the RA system, which should be aimed at addressing a number of these unanswered questions.

Acknowledgments

The present study was partly supported by Grants-in-aid for Scientific Research and for the 21st Century COE Program (Life Science) from MEXT, Japan. We are grateful to Takeda Pharmaceutical Company Limited for kindly providing CV-11974.

References

[1] V.J. Dzau, D.W. Burt, R.E. Pratt, Molecular biology of the renin–angiotensin system, Am. J. Physiol. 255 (1988) F563–F573.
[2] S. Oparil, E. Haber, The renin–angiotensin system (first of two parts), N. Engl. J. Med. 291 (1974) 389–401.
[3] D.J. Campbell, Circulating and tissue angiotensin systems, J. Clin. Invest. 79 (1987) 1–6.
[4] C. Fischer-Ferraro, V.E. Nahmod, D.J. Goldstein, S. Finkielman, Angiotensin and renin in rat and dog brain, J. Exp. Med. 133 (1971) 353–361.
[5] M. Miyazaki, S. Takai, Tissue angiotensin II generating system by angiotensin-converting enzyme and chymase, J. Pharmacol. Sci. 100 (2006) 391–397.
[6] C.H. Block, R.A. Santos, K.B. Brosnihan, C.M. Ferrario, Immunocytochemical localization of angiotensin-(1–7) in the rat forebrain, Peptides 9 (1988) 1395–1401.
[7] R.A. Santos, K.B. Brosnihan, M.C. Chappell, J. Pesquero, C.L. Chernicky, L.J. Greene, C.M. Ferrario, Converting enzyme activity and angiotensin metabolism in the dog brainstem, Hypertension 11 (Suppl. I) (1988) I-153–I-157.
[8] I.F. Benter, D.I. Diz, C.M. Ferrario, Cardiovascular actions of angiotensin(1–7), Peptides 14 (1993) 679–684.
[9] W.B. Campbell, S.N. Brooks, W.A. Pettinger, Angiotensin II- and angiotensin III-induced aldosterone release *in vivo* in the rat, Science 184 (1974) 994–996.
[10] B.D. Nossaman, C.J. Feng, A.D. Kaye, P.J. Kadowitz, Analysis of responses to ANG IV: effects of PD-123319 and DuP-753 in the

pulmonary circulation of the rat, Am. J. Physiol. 268 (1995) L302–L308.

[11] R. Ardaillou, Active fragments of angiotensin II: enzymatic pathways of synthesis and biological effects, Curr. Opin. Nephrol. Hypertens. 6 (1997) 28–34.

[12] R. Kageyama, H. Ohkubo, S. Nakanishi, Primary structure of human preangiotensinogen deduced from the cloned cDNA sequence, Biochemistry 23 (1984) 3603–3609.

[13] H. Ohkubo, R. Kageyama, M. Ujihara, T. Hirose, S. Inayama, S. Nakanishi, Cloning and sequence analysis of cDNA for rat angiotensinogen, Proc. Natl. Acad. Sci. USA 80 (1983) 2196–2200.

[14] K. Kitamura, Y. Ichiki, M. Tanaka, M. Kawamoto, J. Emura, S. Sakakibara, K. Kangawa, H. Matsuo, T. Eto, Immunoreactive adrenomedullin in human plasma, FEBS Lett. 341 (1994) 288–290.

[15] Y. Ichiki, K. Kitamura, K. Kangawa, M. Kawamoto, H. Matsuo, T. Eto, Distribution and characterization of immunoreactive adrenomedullin in human tissue and plasma, FEBS Lett. 338 (1994) 6–10.

[16] F. Fyhrquist, P. Soveri, L. Puutula, U.H. Stenman, Radioimmunoassay of plasma renin activity, Clin. Chem. 22 (1976) 250–256.

[17] K. Shimamoto, H. Ishida, Y. Nakahashi, T. Nishitani, S. Hosoda, T. Yokoyama, S. Tanaka, O. Iimura, A very sensitive direct radioimmunoassay system for plasma angiotensin II and its clinical application in various hypertensive diseases, Jpn. Circ. J. 48 (1984) 1228–1235.

[18] Y.N. Cao, K. Kitamura, K. Ito, J. Kato, S. Hashida, K. Morishita, T. Eto, Glycine-extended adrenomedullin exerts vasodilator effect through amidation in the rat aorta, Regul. Pept. 113 (2003) 109–114.

[19] Y. Ishiyama, K. Kitamura, Y. Ichiki, S. Nakamura, O. Kida, K. Kangawa, T. Eto, Hemodynamic effects of a novel hypotensive peptide, human adrenomedullin, in rats, Eur. J. Pharmacol. 241 (1993) 271–273.

[20] K. Kangawa, H. Matsuo, Purification and complete amino acid sequence of α-human atrial natriuretic polypeptide (α-hANP), Biochem. Biophys. Res. Commun. 118 (1984) 131–139.

[21] A. Miyata, K. Kangawa, T. Toshimori, T. Hatoh, H. Matsuo, Molecular forms of atrial natriuretic polypeptides in mammalian tissues and plasma, Biochem. Biophys. Res. Commun. 129 (1985) 248–255.

[22] I.A. Reid, B.J. Morris, W.F. Ganong, The renin–angiotensin system, Annu. Rev. Physiol. 40 (1978) 377–410.

[23] V.J. Dzau, J.R. Ingelfinger, R.E. Pratt, Regulation of tissue renin and angiotensin gene expressions, J. Cardiovasc. Pharmacol. (Suppl. 10) (1986) S11–S16.

[24] D.J. Campbell, J.F. Habener, Angiotensinogen gene is expressed and differentially regulated in multiple tissues of the rat, J. Clin. Invest. 78 (1986) 31–39.

[25] L.A. Cassis, J. Saye, M.J. Peach, Location and regulation of rat angiotensinogen messenger RNA, Hypertension 11 (1988) 591–596.

THE JOURNAL OF BIOLOGICAL CHEMISTRY VOL. 281, NO. 11, pp. 7129–7135, March 17, 2006
© 2006 by The American Society for Biochemistry and Molecular Biology, Inc. Printed in the U.S.A.

Fyn Is Required for Haloperidol-induced Catalepsy in Mice*

Received for publication, October 26, 2005, and in revised form, December 21, 2005 Published, JBC Papers in Press, January 10, 2006, DOI 10.1074/jbc.M511608200

Kotaro Hattori[‡§¶‖1], Shigeo Uchino[‡‡], Tomoko Isosaka[‡‖**], Mamiko Maekawa[§], Masaomi Iyo[¶], Toshio Sato[¶], Shinichi Kohsaka[‡‡], Takeshi Yagi[‖**§§], and Shigeki Yuasa[‡§]**

*From the [‡]Department of Ultrastructural Research and the [‡‡]Department of Neurochemistry, National Institute of Neuroscience, National Center of Neurology and Psychiatry, Tokyo 187-8502, the [§]Department of Anatomy and Developmental Biology and the [¶]Department of Psychiatry, University Graduate School of Medicine, Chiba 260-8670, [‖]KOKORO Biology Group, FBS, Osaka University, Suita 565-0871, **CREST, Japan Science and Technology Agency, Kawaguchi-shi 332-0012, and [§§]Laboratory of Neurobiology and Behavioral Genetics, National Institute for Physiological Sciences, Okazaki 444-8585, Japan*

Fyn-mediated tyrosine phosphorylation of *N*-methyl-D-aspartate (NMDA) receptor subunits has been implicated in various brain functions, including ethanol tolerance, learning, and seizure susceptibility. In this study, we explored the role of Fyn in haloperidol-induced catalepsy, an animal model of the extrapyramidal side effects of antipsychotics. Haloperidol induced catalepsy and muscle rigidity in the control mice, but these responses were significantly reduced in Fyn-deficient mice. Expression of the striatal dopamine D_2 receptor, the main site of haloperidol action, did not differ between the two genotypes. Fyn activation and enhanced tyrosine phosphorylation of the NMDA receptor NR2B subunit, as measured by Western blotting, were induced after haloperidol injection of the control mice, but both responses were significantly reduced in Fyn-deficient mice. Dopamine D_2 receptor blockade was shown to increase both NR2B phosphorylation and the NMDA-induced calcium responses in control cultured striatal neurons but not in Fyn-deficient neurons. Based on these findings, we proposed a new molecular mechanism underlying haloperidol-induced catalepsy, in which the dopamine D_2 receptor antagonist induces striatal Fyn activation and the subsequent tyrosine phosphorylation of NR2B alters striatal neuronal activity, thereby inducing the behavioral changes that are manifested as a cataleptic response.

Typical antipsychotic agents, such as haloperidol and chlorpromazine, have extrapyramidal side effects (EPS)[2] that resemble Parkinson disease. Drug-induced catalepsy, the impairment of movement initiation, in rodents is an animal model of EPS and is mainly caused by blockade of the dopamine D_2 receptor (D_2-R) (1, 2).

Haloperidol-induced responses are also dependent on *N*-methyl-D-aspartate receptor (NMDA-R) activity, because prior administration of the NMDA-R antagonist MK-801 attenuates haloperidol-induced catalepsy (3, 4). D_2-R and NMDA-R are co-expressed in close proximity along the dendrites of medium spiny neurons in the striatum, and they are functionally coupled in terms of controlling extrapyramidal functions (5).

The NMDA-Rs are hetero-oligomeric ligand-gated ion channels composed of a single NR1 subunit and one type of NR2 (A–D) subunit (6). The most abundant receptor subunits in the striatum are NR1, NR2A, and NR2B (7, 8). These three subunits are involved in extrapyramidal functions (5), and we have found that an NR2B-selective antagonist attenuates haloperidol-induced catalepsy (9).

Phosphorylation of tyrosine residues on the NMDA-R has been reported to modulate its channel characteristics (10, 11). Depriving the striatum of dopaminergic input increases the tyrosine phosphorylation of the striatal NMDA-R and the motor response (12, 13), but infusing the striatum with a tyrosine kinase inhibitor, genistein, attenuates both the tyrosine phosphorylation and the motor response induced by dopaminergic deprivation (13).

Fyn is a member of the Src family kinases (SFKs) and is associated with the NMDA-R at postsynaptic densities. Fyn phosphorylates NMDA-R subunits and modifies their channel activity (14). One of the NMDA-R subunits, NR2B, is preferentially phosphorylated by Fyn, and its phosphorylation has been implicated in several brain functions, including ethanol tolerance, long term potentiation, and seizure susceptibility (15–18). The Tyr-1472 of NR2B is a particularly key site for Fyn-mediated phosphorylation (17, 19).

To investigate the role of Fyn in the cataleptic behavior induced by haloperidol, we studied these haloperidol effects in Fyn-deficient mice and biochemically analyzed the Fyn-mediated signal transduction initiated by haloperidol. Based on our results, we discuss the significance of Fyn activation in haloperidol-induced catalepsy within the scope of signal transduction from D_2-R inhibition to modulation of the extrapyramidal system.

MATERIALS AND METHODS

Animals—Fyn tyrosine kinase-deficient mice were generated by inserting the β-galactosidase gene (*lacZ*) into the reading frame of the *fyn* gene as described previously (20). Because the *lacZ* introduced is expressed in both heterozygous ($+/fyn^Z$) and homozygous (fyn^Z/fyn^Z) mice, heterozygous mice were mainly used as the controls instead of wild-type mice to compensate for the possible effect of *lacZ* expression as a foreign gene. The background of this mutant's strain is C57BL/6J. Genotypes were analyzed by the PCR. All animals were maintained under standard laboratory conditions as described previously (15). All experimental procedures were in accordance with the 1996 National Institutes of Health guidelines and were approved by the Animal Care Committee of the Chiba University Graduate School of Medicine,

* This work was supported in part by Ministry of Health, Labor, and Welfare of Japan Research Grants 9B-4 and 15B-3 for Nervous and Mental Disorders, the Futaba Electronics Memorial Foundation, the Program for Promotion of Fundamental Studies in Health Sciences of the National Institute of Biomedical Innovation Grant 05-32, and Long Range Research Initiative by Japan Chemical Industry Association (to S. Y.). The costs of publication of this article were defrayed in part by the payment of page charges. This article must therefore be hereby marked "*advertisement*" in accordance with 18 U.S.C. Section 1734 solely to indicate this fact.

The on-line version of this article (available at http://www.jbc.org) contains Figs. S1 to S5.

[1] To whom correspondence should be addressed: Dept. of Ultrastructural Research, National Institute of Neuroscience, National Center of Neurology and Psychiatry, Tokyo 187-8502, Japan. Tel.: 81-42-346-1719; Fax: 81-42-346-1749; E-mail: hattori@ncnp.go.jp.

[2] The abbreviations used are: EPS, extrapyramidal side effects; BSS, balanced salt solution; D_2-R, dopamine D_2-receptor; HAL, Haloperidol; NMDA, *N*-methyl-d-aspartate; NMDA-R, *N*-methyl-d-aspartate receptor; PKA, protein kinase A; PKC, protein kinase C; SFKs, Src family kinases; TBS, Tris-buffered saline; TH, tyrosine hydroxylase.

Osaka University, and the National Institute of Neuroscience, National Center of Neurology and Psychiatry.

Pharmacological Agents—Haloperidol, the dopamine D_2-R-selective antagonist L-741,626 (21), and the D_2-R-selective agonist (−)-quinpirole were purchased from Sigma. The drugs were administered by intraperitoneal injection in a volume of 10 μl/g body weight. All solutions were prepared immediately prior to the experiments. To exclude the effect of drug tolerance, no animals were used more than once in the pharmacological experiments.

Antibodies—Goat polyclonal anti-D_2-R antibody (N19) was purchased from Santa Cruz Biotechnology (Santa Cruz, CA). Rabbit polyclonal anti-tyrosine hydroxylase (TH) antibody was obtained from Chemicon (Temecula, CA). A mouse monoclonal anti-phosphotyrosine antibody (Tyr(P)-100) was purchased from Cell Signaling Technology (Beverly, MA). Phosphorylation site-specific rabbit polyclonal antibody against p-Src (Y418) and p-Src (Y529) was obtained from BIOSOURCE (Camarillo, CA) and against p-NR2B (Y1472) was from Sigma. Rabbit polyclonal anti-NR2B antibody was a gift from Dr. Masahiko Watanabe (22). Anti-Src mouse monoclonal antibody (GD11) was purchased from Upstate Biotechnology, Inc. (Lake Placid, NY). The anti-Fyn rat monoclonal antibody (γC3) was raised by Dr. Masahiro Yasuda (23). The anti-βIII tubulin mouse monoclonal antibody was purchased from Promega (Madison, WI).

Assessment of Catalepsy—Catalepsy was measured by a bar test (24). The test was carried out 1 h after intraperitoneal injection of haloperidol (0–1.0 mg/kg) or L-741,626 (0–10 mg/kg). A 3-mm-diameter wooden bar was fixed horizontally 4 cm above the floor of a Plexiglas cage. The animals were placed inside the test cage and allowed to acclimatize for 5 min prior to performing the bar test. Both forepaws were then gently placed on the bar, and the length of time during which each mouse maintained the initial position was measured (maximum cut-off time, 180 s).

Analysis of Rigidity—Muscle rigidity after haloperidol administration was assessed by a mechanographic technique using a modified device designed for rat experiments (25). The mouse was placed in a narrow, well ventilated plastic tube to restrict body movement, and one hind leg was bound to a force sensor (AD4937-5N, A & D Co. Ltd., Tokyo, Japan) that records linear reciprocating motion (15-mm distance, 15 cycles/min) via a crank and motor. The raw data from the force sensor were analyzed on a Macintosh computer connected to an A/D converter and software (PowerLab 4s, chart version 3.6 ADInstruments, Mountain View, CA), and the resistance of the flexor and extensor muscles to forced extension and flexion of the knee and ankle joint was measured. The mice were attached to the above device, and the difference in muscle resistance before and after the administration of vehicle or haloperidol (1.0 mg/kg) was recorded. The mean amplitude of 10 consecutive waves at each time point was calculated. Spikes that indicated spontaneous movements of the mice were excluded from the count.

In Situ Hybridization Histochemistry—The distribution of D_2-R gene expression in the striatum of the control and Fyn-deficient mice was compared. The probe was prepared as follows. A cDNA fragment encoding the sequence of mouse D_2-R (1.3 kbp, a gift from Dr. T. Kaneko, Kyoto University) was cloned into the pBluescript II/KS− vector, and the clone was digested and used as a DNA template to synthesize an antisense or sense digoxigenin-labeled cRNA probe. The probe was prepared with T7 or T3 RNA polymerase and a digoxigenin RNA labeling kit (Roche Applied Science). Staining was performed as reported previously (26). The sense cRNA probe was employed as the control, and no signals in the brain were detected with it.

Immunoblot Analysis—One hour after administration of the vehicle, haloperidol (1.0 mg/kg), or L-741,626 (5 mg/kg), the striatum was immediately dissected and frozen in liquid nitrogen. The striatum was placed in buffer containing 10% sucrose, 3% SDS, 10 mM Tris-HCl, pH 6.8, 1 mM sodium orthovanadate, and 1 mM phenylmethylsulfonyl fluoride and homogenized with a Polytron homogenizer (Kinematica AG, Lucerne, Switzerland). Samples were spun down (20,000 × *g*, 15 min) to remove insoluble material, and the protein concentration was determined with the BCA protein assay reagent (Pierce). After the addition of 40 mM dithiothreitol, the samples were boiled for 5 min, and an equal amount of protein (40 μg per lane) from each sample was separated by electrophoresis on 10% polyacrylamide gels. The gels were transferred onto Immobilon membranes (Millipore, Bedford, MA). The membranes were blocked with 1% bovine serum albumin in Tris-buffered saline (TBS; pH 7.5) containing 0.1% Tween 20 (TBS-T) or 10% skim milk in TBS-T for 1 h and probed with primary antibodies (1:750 dilution for TH, 1:4000 for anti-βIII tubulin, and 1:1000 for other antibodies). After washing three times with TBS-T, the membranes were incubated with horseradish peroxidase-labeled secondary antibodies (anti-goat, anti-rabbit, anti-rat, or anti-mouse IgG, 1:20,000 dilution, all purchased from The Jackson Laboratories, West Grove, PA). After washing three times, the signals were detected with ECL Plus (Amersham Biosciences) and ATTO Cool Saver (ATTO Corp., Tokyo, Japan). The membranes were then incubated with stripping buffer (100 mM 2-mercaptoethanol, 2% SDS, 62.5 mM Tris-HCl, pH 6.7) at 50 °C for 30 min, washed, blocked, and reprobed with other antibodies.

Immunoprecipitation and Western Blotting—The procedures for immunoprecipitation were as described previously (15). Striatum obtained 1 h after vehicle or haloperidol (1.0 mg/kg) administration was placed in lysis buffer (10 mM Tris-HCl, pH 7.4, 1% Triton X-100, 0.1% sodium deoxycholate, 0.1% SDS, 0.15 M NaCl, 1 mM EDTA, and 1 mM sodium orthovanadate) and homogenized with a Polytron homogenizer. Samples were spun down to remove insoluble material, and the protein concentration was determined. Equal amounts of protein (500 μg) were then used for immunoprecipitation. Samples were precleared with protein G-Sepharose (Amersham Biosciences), incubated for 1 h at 4 °C with 1 μg of the anti-Fyn or anti-Src antibody, and then incubated for 1 h at 4 °C with 10 μl of protein G-Sepharose. After three washes with lysis buffer, the pelleted protein G-Sepharose was boiled for 5 min in 30 μl of SDS sample buffer, and 15 μl of the supernatant was subjected to SDS-PAGE. The separated proteins were subsequently blotted onto Immobilon, probed with each antibody, and visualized as described above.

Primary Cultures of Striatal Neurons—Primary cultures of striatal neurons were prepared from the fetal striata of wild-type and Fyn-deficient mice at embryonic day 17. Striata from 6 to 8 fetal brains were dissected and placed in Hanks' balanced salt solution (Invitrogen) and then were transferred into a dissociation medium containing Hanks' balanced salt solution, 0.05% DNase I, and 1% trypsin/EDTA and incubated at 37 °C for 7 min. After sedimentation, the supernatant was removed, and the pellet was washed three times with Hanks' balanced salt solution containing 1% penicillin/streptomycin. The tissue was gently placed in Hanks' balanced salt solution containing 0.05% DNase I and triturated with a plastic pipette until a homogeneous suspension was obtained. After centrifugation at 130 × *g* for 8 min, the cell pellet was resuspended in Neurobasal/B27 medium (Invitrogen) containing 0.5 mM L-glutamine and penicillin/streptomycin (100 units/ml). The cell cultures were seeded at a density of 3×10^5 cells/cm^2 on 0.1% polyethyleneimine-coated cover glasses in 1.9 cm^2/well dishes (Nunclon, Nunc). Cells were maintained at 37 °C under a humidified 5% CO_2

atmosphere. The cultured striatal neurons were identified immunocytochemically with anti-GAD65 antibody (Chemicon) and anti-MAP2 antibody (Sigma). More than 95% of both the wild-type and Fyn-deficient neurons were double-labeled by anti-GAD65 and anti-MAP2 (supplemental Fig. S1).

Calcium Imaging—Calcium imaging was carried out as described previously (27). Briefly, striatal primary cells were incubated with 10 μM fura-2/AM (Dojindo) for 1 h at 30 °C in balanced salt solution (BSS) consisting of (in mM) NaCl 130, KCl 5.4, glucose 5.5, HEPES 10, and $CaCl_2$ 2, and adjusted to pH 7.4 with NaOH. After washing, the cover glasses that contained cultured neurons were mounted on the stage of an inverted fluorescence microscope (IX50; Olympus) and perfused with BSS at a flow rate of 1.8 ml/min. The perfusion medium was pre-warmed and maintained at 32.6 ± 1.1 °C in the measurement dish. Fluorescence images obtained by alternate excitation with 340 and 380 nm light through the ×20 objective lens and CCD camera (C2400-8; Hamamatsu Photonics, Hamamatsu, Japan) were fed into an image processor (Argus 50, Hamamatsu) for ratiometric analysis. The effect of the D_2-R antagonist L-741,626 on the channel activity of NMDA receptors was investigated in the presence of the selective D_2-R agonist quinpirole in the perfusion medium. As shown in supplemental Fig. S2, quinpirole alone had a dose-dependent inhibitory effect on the channel activity of the NMDA receptors of the striatal primary neurons of the control mice consistent with its inhibitory effect reported in the striatal slice culture (28). Quinpirole was observed to have almost the same degree of the inhibitory effect on Fyn-deficient neurons (49% decrease at 50 μM).

Preparation of Protein Samples from the Cultured Neurons—Striatal neurons were cultured in 1.9 cm^2/well dishes (Nunclon, Nunc) as described above. Each solution used in the following experiments was pre-warmed to 37 °C in a water bath. Culture dishes were warmed on a heat block to 37 °C. The culture medium was removed, and the cultured cells were incubated with BSS for at least 5 min. The cells were then incubated with the following: 1) BSS for 7 min followed by incubation in quinpirole (50 μM) in BSS for 7 min, or 2) in quinpirole (50 μM) in BSS for 7 min followed by a mixture of quinpirole (50 μM) and L-741,626 (10 μM) in BSS for 7 min. The solution was removed, and the cells were immediately lysed in 150 μl of SDS sample buffer.

Statistical Analyses—The results of the catalepsy assessment and calcium imaging were evaluated by the Kruskal-Wallis test followed by the Mann-Whitney *U* test. The results of the muscle rigidity analysis were evaluated by a two-way repeated measure ANOVA. The results of Western blotting were evaluated by one-way ANOVA followed by Bartlett's test. All data are expressed as the mean ± S.E.

RESULTS

Haloperidol induced catalepsy in the $+/fyn^Z$ mice, and the duration of the catalepsy increased in a dose-dependent manner (Fig. 1). By contrast, the duration of the catalepsy in the fyn^Z/fyn^Z mice was significantly shorter (Fig. 1). At the 1.0 mg/kg dose, there was no difference in the cataleptic response between the +/fynZ mice and the wild-type mice (154.5 ± 47.1 s). The D_2-R-selective antagonist L-741,626 was confirmed to induce catalepsy in the control mice (supplemental Fig. S3), as reported previously in rats (29), but the duration of the catalepsy was significantly reduced in fyn^Z/fyn^Z mice (supplemental Fig. S3). Because there was no significant difference in the temporal patterns of the locomotor activity between $+/fyn^Z$ mice and fyn^Z/fyn^Z mice (30), the altered cataleptic response in the fyn^Z/fyn^Z mice was concluded not to be due to a locomotion defect.

Because Fyn-deficient mice are more fearful than control mice (31), we suspected that they might avoid a procedure like the "bar test" and that the duration of catalepsy would be misleadingly short as a result. We therefore also measured muscular rigidity to minimize any such emotional influence on the response to haloperidol. Haloperidol induced a marked increase in hind limb muscle rigidity in the $+/fyn^Z$ mice that was detectable as early as 45 min after administration (1.0 mg/kg) and persisted for more than 2 h, but no increase in muscle rigidity was detected in the fyn^Z/fyn^Z mice (Fig. 2 and supplemental Fig. S4).

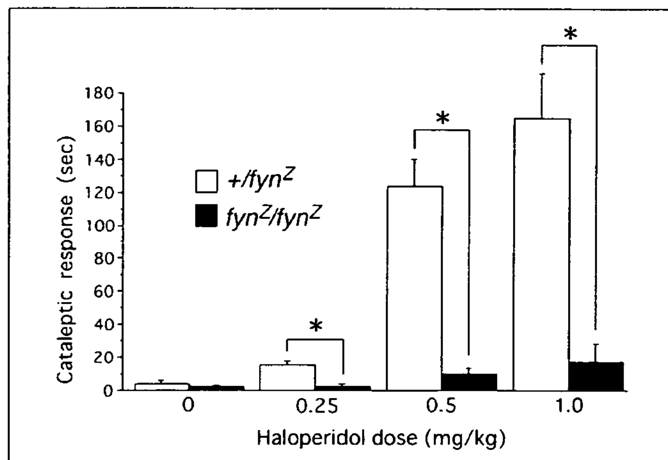

FIGURE 1. **Assessment of catalepsy following haloperidol administration.** The cataleptic response to haloperidol administration increased dose-dependently in $+/fyn^Z$ mice but was significantly reduced in fyn^Z/fyn^Z mice. Eight to twelve animals were used in each group. The *columns* represent the means, and the *bars* represent the S.E. Statistically significant differences were identified by the Mann-Whitney *U* test; *, $p < 0.001$.

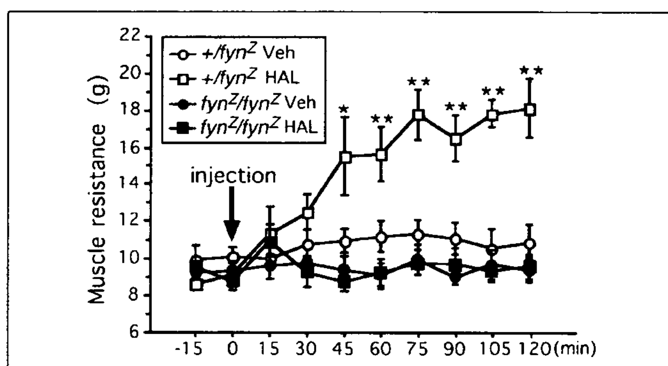

FIGURE 2. **Mean amplitude of muscle resistance before and after haloperidol (*HAL*) injection.** In $+/fyn^Z$ mice, muscular rigidity increased as early as 45 min after haloperidol administration (1 mg/kg), and the increase persisted for more than 2 h. By contrast, no increase in muscle rigidity was detected in the fyn^Z/fyn^Z mice after haloperidol administration. Administration of vehicle (*Veh*) alone did not affect rigidity in either genotype. Six animals were used in each group. Data are expressed as means ± S.E. Statistically significant differences were identified by two-way repeated measure ANOVA; *, $p < 0.05$; **, $p < 0.005$.

To exclude the possibility that the failure to respond to haloperidol was because of a difference in D_2-R expression, *in situ* hybridization of D_2-R mRNA and Western blotting of D_2-R protein were performed on the striatum of $+/fyn^Z$ and fyn^Z/fyn^Z mice. As shown in Fig. 3, no clear difference was observed in either striatal D_2-R gene expression (Fig. 3*A*) or the protein level (Fig. 3*B*). Western blotting analysis of striatal TH was also performed to determine whether there was any difference between the two genotypes in the abundance of the rate-limiting enzyme in dopamine biosynthesis, but little difference in the amount of TH protein was found (Fig. 3*C*).

The effect of haloperidol on protein tyrosine phosphorylation in the

striatum of the $+/fyn^Z$ and fyn^Z/fyn^Z mice was compared by Western blotting. One hour after haloperidol administration (1.0 mg/kg), a marked increase in tyrosine phosphorylation of several proteins, including 60-, 110-, and 180-kDa proteins, was observed in the striatum of the $+/fyn^Z$ mice but not of the fyn^Z/fyn^Z mice (Fig. 4*A*).

Because the 60-kDa protein corresponds in size to SFKs, we measured tyrosine phosphorylation of the activation-related Tyr-418 residue on SFKs. As shown in Fig. 4*B*, phospho-Tyr-418 increased after haloperidol injection of the $+/fyn^Z$ mice, but no such effect was observed in the fyn^Z/fyn^Z mice. Basal Tyr(P)-418 immunoreactivity was much lower in the fyn^Z/fyn^Z mice. Because the anti-pY418 antibody recognizes both

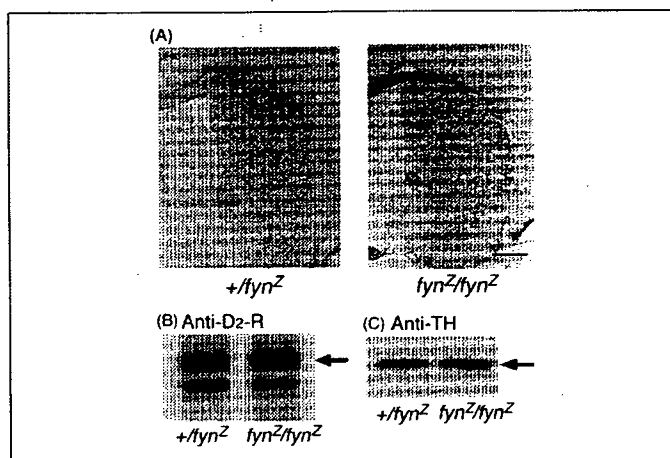

FIGURE 3. **Expression of dopaminergic markers in the striatum.** *A*, *in situ* hybridization histochemistry for dopamine D_2 receptor mRNA. Strong D_2 receptor expression in the striatum was seen in both genotypes, and there was little difference in its distribution. *Scale bar*, 500 μm. *B*, Western blotting analysis of the dopamine D_2 receptor in the striatum. The intensity of the upper band (*arrow*) around 85 kDa, corresponding to the D_2-receptor, was essentially the same in both genotypes. *C*, Western blotting analysis of striatal tyrosine hydroxylase (*TH*). The intensity of the band at around 70 kDa differed little between the two genotypes.

Fyn and Src, we immunoprecipitated Fyn and Src, and we examined the phosphorylation of the activation-related residue, Tyr-418, and of the inhibition-related residue, Tyr(P)-529, by Western blotting in the $+/fyn^Z$ mice. As shown in Fig. 4*C*, Fyn but not Src was activated at Tyr-418 by haloperidol, and no change was observed in the phosphorylation at Tyr-529. Because the 180-kDa protein corresponds in size to the NR2B subunit, we also measured the phosphorylation of the Tyr-1472 of NR2B, the key phosphorylation site, by Fyn. The results showed that phospho-Tyr-1472 increased in the $+/fyn^Z$ mice but not in the fyn^Z/fyn^Z mice (Fig. 4*D*). The basal level of Tyr(P)-1472 in the fyn^Z/fyn^Z mice was not significantly different from the basal level in the $+/fyn^Z$ mice. Marked increases in tyrosine phosphorylation of the 60-, 110-, and 180-kDa proteins and up-regulation of Tyr(P)-418 and Tyr(P)-1472 were also observed following L-741,626 administration to the control mice, but no such effects were observed in the fyn^Z/fyn^Z mice (supplemental Fig. S5).

There were no sex differences in the results of either the behavioral or biochemical studies (data not shown). The same findings in regard to the haloperidol-induced enhancement of tyrosine phosphorylation were also observed in the wild-type mice, and no clear difference was detected between $+/fyn^Z$ mice and wild-type mice (data not shown). To investigate whether the Fyn-mediated increase in NMDA receptor phosphorylation by D_2-R blockade affects NMDA receptor activity, we prepared striatal primary cultures and assessed the channel activity of NMDA receptors by the calcium imaging method.

After 4–7 days of culture, we loaded 10 μM fura-2/AM into the primary cells and measured the increase in intracellular calcium concentration ($[Ca^{2+}]_i$) by calcium fluorimetry. Exposure to 3 μM NMDA/10 μM glycine for 30 s induced a robust response in more than 95% of the cells analyzed, and repeated applications of NMDA/glycine at 5-min intervals evoked reproducible responses (data not shown), indicating little desensitization of the NMDA receptors under our experimental conditions.

We first examined the effect of a D_2-R-selective antagonist,

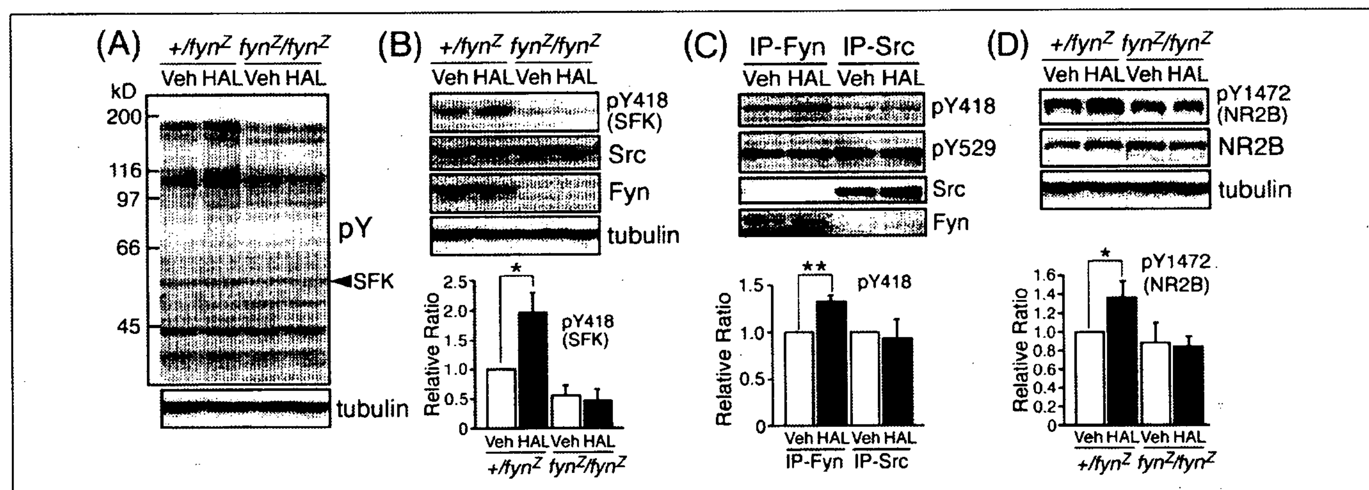

FIGURE 4. **Tyrosine phosphorylation in the striatum after haloperidol administration.** *A*, haloperidol (*HAL*) administration (1.0 mg/kg) increased the tyrosine phosphorylation of several proteins, including 60-, 110-, and 180-kDa proteins, in $+/fyn^Z$ mice compared with vehicle (*Veh*) administration, but no such difference was found in the fyn^Z/fyn^Z mice. *B*, the same tendency toward a haloperidol-induced increase in tyrosine phosphorylation was observed in regard to Tyr-418 of Src family kinases (pY418) in the $+/fyn^Z$ mice, but no such increase was observed in the fyn^Z/fyn^Z mice. The amounts of Src and Fyn were unchanged. Densitometric analysis revealed a significant increase in the band density of the Tyr(P)-418 of Src family kinases after injection in $+/fyn^Z$ mice with haloperidol. No such increase was detected in the fyn^Z/fyn^Z mice, and the basal band density was also much lower in fyn^Z/fyn^Z mice. *C*, haloperidol-induced increase in the phosphorylation of the Src family kinases Src and Fyn in the control mice demonstrated by immunoprecipitation (*IP*) and Western blotting. Haloperidol (1.0 mg/kg) induced an increase in Tyr(P)-418 following anti-Fyn immunoprecipitation but not following anti-Src immunoprecipitation. No clear change was observed in Tyr(P)-529. The amounts of Src and Fyn were unchanged. Densitometric analysis revealed an increase after haloperidol injection in the band of Tyr(P)-418 on Fyn but not Src. *D*, there was also a significant increase in the band density of Tyr(P)-1472 on NR2B following haloperidol injection in $+/fyn^Z$ mice. No such difference was detected in the fyn^Z/fyn^Z mice. The basal level of Tyr(P)-1472 in the fyn^Z/fyn^Z mice tended to decrease in comparison with the $+/fyn^Z$ mice, but the difference was not significant. The amount of NR2B was unchanged. *HAL*, haloperidol (1.0 mg/kg); *Veh*, vehicle. Four to six animals were used in each group. The *columns* represent means, and the *bars* represent means ± S.E. One-way ANOVA; *, $p < 0.01$; **, $p < 0.05$.

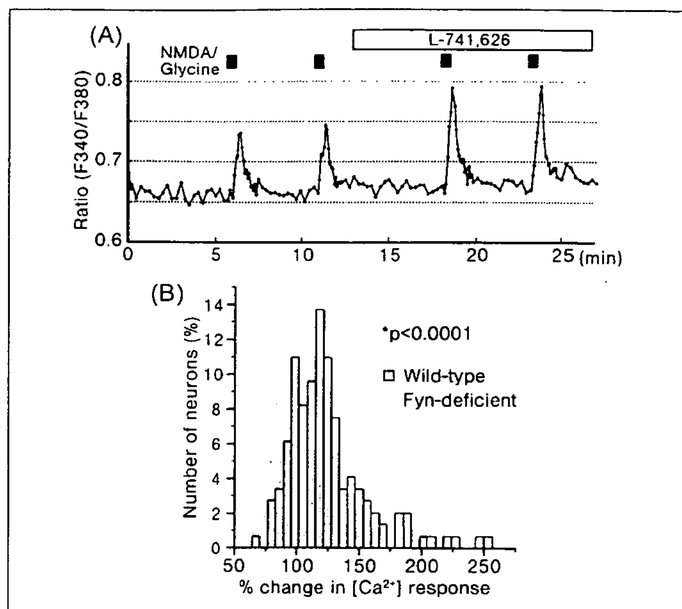

FIGURE 5. **Effect of a D_2-R selective antagonist, L-741,626, on the channel activity of NMDA receptors in primary striatal neurons assessed by Ca^{2+} fluorimetry.** *A*, $[Ca^{2+}]_i$ responses of wild-type neurons in the presence of quinpirole (50 μM). A representative trace of wild-type neurons exposed to two applications of 3 μM NMDA, 10 μM glycine (control response) and two applications of 3 μM NMDA, 10 μM glycine 5 min after starting L-741,626 (10 μM) addition to the perfusion buffer. The addition of L-741,626 significantly enhanced NMDA/glycine-induced $[Ca^{2+}]_i$ responses compared with the control responses. *B*, histogram of $[Ca^{2+}]_i$ responses induced by 3 μM NMDA, 10 μM glycine in the presence of L-741,626 (10 μM) relative to those in the absence of L-741,626 (control response). Large numbers (74.7%) of the wild-type neurons (*open bars*) exhibited larger NMDA/glycine-induced $[Ca^{2+}]_i$ responses after the addition of L-741,626 (mean change, 125.7 ± 34.1% of the control responses), whereas the number of Fyn-deficient neurons (*filled bars*) showing larger responses was significantly decreased (46.6%, mean change, 105.8 ± 26.9% of the control responses). There was also a group of Fyn-deficient neurons that exhibited larger responses after L-741,626 addition that peaked at around 120% of the control responses. Eight wild-type and six Fyn-deficient striatal neuronal cultures were used. Mann-Whitney *U* test.

L-741,626, on the channel activity of NMDA receptors of wild-type neurons in the presence of a D_2-R-selective agonist, quinpirole (50 μM). After confirming that the responses evoked were reproducible by two successive applications of 3 μM NMDA, 10 μM glycine (control responses), we added 10 μM L-741,626 to the perfusion buffer BSS. After 5 min, we measured the 3 μM NMDA, 10 μM glycine-induced increases in $[Ca^{2+}]_i$ and compared them with the control responses. As shown in Fig. 5*A*, larger responses than the control responses were detected in the presence of L-741,626, but in some neurons, almost identical responses were observed both in the presence and absence (control) of L-741,626. The distribution of changes in $[Ca^{2+}]_i$ responses after the addition of L-741,626 is shown in Fig. 5*B* (*open bars*). After the addition of L-741,626, a large number of neurons (74.7%) showed larger responses than the control responses (mean change, 125.7 ± 34.1%).

To determine whether the larger NMDA/glycine-induced responses induced by L-741,626 were mediated by Fyn, we performed the same experiments on primary cultures prepared from Fyn-deficient mice. After the addition of L-741,626, only 46.6% of the Fyn-deficient neurons showed larger responses than the control responses, and L-741,626 addition had little enhancing effect on the responses (mean change, 106.8 ± 26.9% of the control responses; see Fig. 5*B*, *filled bars*). A subset of Fyn-deficient neurons exhibited larger responses after L-741,626 addition, and their responses peaked at around 120% of the control responses. In addition, the numbers of neurons exhibiting larger responses after L-741,626 addition was lower in the presence of the Src family inhibitor PP2 (10 μM) (mean change, 99.9 ± 15.7% of the control responses).

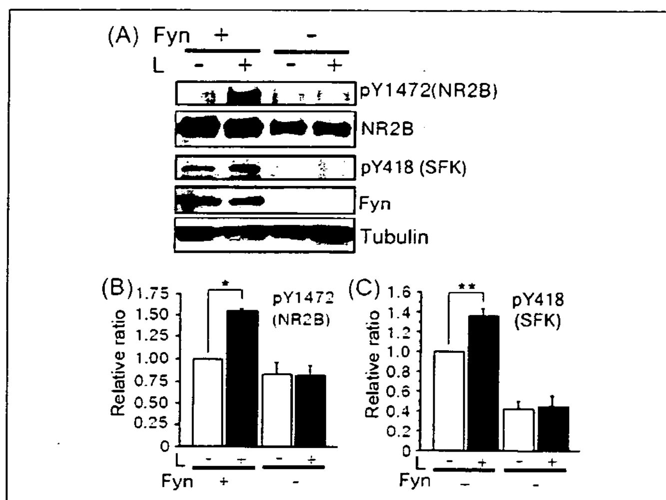

FIGURE 6. **Western blot analysis of striatal primary neurons.** *A*, neurons were exposed to or not exposed to L-741,626 (10 μM) in the presence of quinpirole. L-741,626 (10 μM) markedly increased the tyrosine phosphorylation at Tyr-1472 of NR2B (*pY1472*) and at Tyr-418 of Src family kinases (*pY418*) in the wild type, but no such difference was found in Fyn deficiency. *B*, densitometric analysis revealed a significant increase in the band density of the Tyr(P)-1472 of NR2B in the wild type. No such increase was detected in Fyn deficiency. *C*, there was also a significant increase in the band density of the Tyr(P)-418 of the Src family kinases when L-741,626 was added to the wild type. No such difference was detected in Fyn deficiency. Six wild-type and six Fyn-deficient striatal neuronal cultures were used. The *columns* represent means, and the *bars* represent S.E. One-way ANOVA; *, $p < 0.0001$; **, $p < 0.005$.

We then examined the effect of L-741,626 on Fyn activation and NMDA receptor phosphorylation in the presence of quinpirole (50 μM) by Western blot analysis, as shown in Fig. 6. Primary cells were exposed or not exposed (control) to 10 μM L-741,626 for 7 min prior to sample preparation. In the wild-type cells, immunoreactivity for anti-pY1472 antibody and anti-pY418 antibody in the L-741,626-treated cell extracts was stronger than in the control cell extracts. By contrast, when Fyn-deficient cells were used, there were no significant differences in immunoreactivity for anti-pY1472 antibody and anti-pY418 antibody between the L-741,626-exposed cell extracts and the control cell extracts.

DISCUSSION

The results of this study show that Fyn is required for haloperidol-induced catalepsy. We also found that haloperidol induces Fyn activation and a Fyn-dependent increase in NR2B phosphorylation in mouse striatum. We used striatal primary neurons to verify that D_2-R blockade induced Fyn activation, enhancement of NR2B phosphorylation, and potentiation of the channel activity of NMDA receptor at the cellular level, and the latter two effects were significantly reduced in Fyn-deficient neurons. On the basis of these findings, we propose a new molecular mechanism that underlies haloperidol-induced catalepsy in which the D_2-R antagonist induces Fyn activation in the striatum, and the subsequent phosphorylation of the NR2B subunit by the activated Fyn increases the channel activity of NMDA receptors, which leads to changes in neural transmission and results in the cataleptic response.

Because haloperidol-induced catalepsy and muscular rigidity are mainly caused by blockade of dopamine D_2-Rs in the striatum (1, 2), sensitivity to haloperidol should be altered by changes in dopaminergic transmission. However, there were no clear differences between Fyn-deficient mice and control mice in the expression pattern of the D_2-R gene or the amounts of D_2-R protein and tyrosine hydroxylase, and measurements by microdialysis showed no significant difference in striatal basal dopamine levels (32). Thus, it is rather unlikely that the

reduced sensitivity to haloperidol in the Fyn-deficient mice is because of defective dopaminergic transmission.

We found that haloperidol increased phosphorylation of the Tyr-418 residues of Fyn. The catalytic activity of SFKs is controlled through autocatalytic phosphorylation and dephosphorylation, particularly at amino acid residues Tyr-418 and Tyr-529 (14), and the phosphorylated Tyr-529 intramolecularly interacts with an Src homology 2 domain to form a loop, thereby suppressing kinase function. Intermolecular autophosphorylation at Tyr-418, on the other hand, activates SFKs by displacing Tyr-418 from the substrate-binding site, thus allowing the kinase to gain access to substrates (33). We found that the haloperidol-induced increase in Tyr-418 phosphorylation occurred specifically in Fyn and did not occur in Src, whereas phosphorylation of Tyr-529 was the same in both Src and Fyn. Thus, Fyn is specifically activated by haloperidol *in vivo*.

Haloperidol also increased the phosphorylation of Tyr-1472 in the NR2B subunit, and because no increase was observed in Fyn-deficient mice, the haloperidol-induced phosphorylation of NR2B subunit must be dependent on Fyn. Moreover, we confirmed this D_2-R antagonist induced Fyn-mediated enhancement of NR2B phosphorylation at the cellular level in primary cultures of striatal neurons.

Fyn-mediated phosphorylation of NR2B and potentiation of NMDA-R channel activity are involved in several brain functions, including ethanol tolerance (15), seizure susceptibility (23), and long term potentiation (17). Activation of EphB receptors has also been reported to result in increased phosphorylation of NR2B and an increase in NMDA-R channel activity measured by Ca^{2+} imaging in hippocampal primary cultures (34). The use of HEK293T cells transfected with a mutant NR2B construct in this study also showed that Fyn-mediated tyrosine phosphorylation of NR2B is required for the increase in NMDA-R channel activity. In our study, NMDA-R channel activity in most wild-type striatal neurons was increased by the blockade of D_2-R, and the proportion of such neurons was significantly reduced in Fyn deficiency. Thus, the increased NMDA-R activity after D_2-R blockade in most of the striatal neurons was Fyn-dependent. However, NMDA-R may also be activated by a Fyn-independent pathway, because a certain proportion of the neurons in the Fyn-deficient striatal culture exhibited increased NMDA-R activity.

It has been repeatedly observed that the NMDA-R antagonist MK-801 attenuates haloperidol-induced catalepsy (9, 35–37), and we recently reported that prior exposure to the NR2B-selective antagonist CP-101,606 significantly reduces haloperidol-induced catalepsy (9). Thus, haloperidol-induced catalepsy is specifically dependent on NR2B function, and activation of NR2B function by Fyn-mediated phosphorylation is likely to be required for catalepsy to occur.

NMDA-R dysfunction is hypothesized to be the pathogenetic mechanism responsible for schizophrenia, because NMDA-R antagonists cause psychotic states resembling schizophrenia (38–40), and mice with reduced NMDA-R expression have been reported to display schizophrenia-related behaviors (41). Because unmedicated schizophrenic patients exhibit attenuated EPS shortly after haloperidol administration compared with healthy controls (42), the lower responsiveness to haloperidol in Fyn-deficient mice may mimic a feature of schizophrenia.

Several mutant mice, including mice deficient in the D_2-R (24), A_{2A}-adenosine receptor (43), retinoid X receptor γ1 (44), and protein kinase A (PKA) (45), show reduced cataleptic responses to haloperidol. The reduced cataleptic response in one of them, the PKA-deficient mutant, is likely to be caused by a molecular mechanism similar to that in Fyn deficiency, because an increase in PKA-mediated serine phosphorylation of striatal NR1 subunits increases following haloperidol administration (46). The scaffolding protein RACK1 binds to both Fyn and NR2B, and the three molecules form a complex in rat hippocampus (16, 47). Dissociation of RACK1 from this RACK1-Fyn-NR2B complex facilitates Fyn-mediated phosphorylation of NR2B (47). Because PKA activation has been demonstrated to dissociate RACK1 from this complex (16), the above PKA-RACK1-Fyn pathway may also exist downstream of D_2-R in the striatum.

Another molecule that may act between D_2-R and Fyn is PKC. Activation of G-protein-coupled receptors, such as muscarinic and metabotropic glutamate receptors, in the hippocampus increases NMDA-evoked currents via protein kinase C (PKC) (48). The increase in NMDA-R function is mediated by the activation of SFKs, because the PKC-induced NMDA-R up-regulation is blocked by an inhibitor of Src and Fyn and does not occur in Src-deficient cells (48). D_2-R is another G-protein-coupled receptor, and because haloperidol administration acutely increases PKC activity in the rat striatum (49), Fyn activation after D_2-R blockade may be mediated by the PKC pathway.

Other molecules, including receptor tyrosine kinases (34, 50) and a cytokine receptor (51), have also been reported to be involved in SFK-mediated phosphorylation and activation of NMDA-R, and they may be involved in the striatal activation of Fyn after D_2-R inhibition.

In this study we found that blockade of D_2-R causes Fyn activation, Fyn-mediated NMDA-R phosphorylation, and potentiation of its channel activity in the striatal neurons that may be responsible for haloperidol-induced catalepsy. Further investigation should focus on the above-postulated Fyn-activation mechanisms initiated by D_2-R blockade, and these transduction steps should be drug targets for controlling not only motor function but higher cognitive brain function.

Acknowledgments—We are grateful to Dr. H. Niki (Brain Science Institute, RIKEN, Japan) for reading the manuscript and giving us invaluable advice. We are also grateful to Dr. T. Kaneko (Kyoto University) for the gift of the mouse dopamine D_2 receptor cDNA, Dr. M. Watanabe (Hokkaido University) for the gift of the anti-NR2B antibody, and Prof. N. Koshikawa (Department of Pharmacology, Nihon University School of Dentistry) for helpful advice on the determination of muscular rigidity. We also thank K. Kamimura and T. Muto (Department of Anatomy and Developmental Biology, Chiba University Graduate School of Medicine) for their technical assistance in the immunohistochemistry and behavioral analyses.

REFERENCES

1. Crocker, A. D., and Hemsley, K. M. (2001) *Prog. Neuropsychopharmacol. Biol. Psychiatry* **25**, 573–590
2. Wadenberg, M. L., Soliman, A., VanderSpek, S. C., and Kapur, S. (2001) *Neuropsychopharmacology* **25**, 633–641
3. Moore, N. A., Blackman, A., Awere, S., and Leander, J. D. (1993) *Eur. J. Pharmacol.* **237**, 1–7
4. Chartoff, E. H., Ward, R. P., and Dorsa, D. M. (1999) *J. Pharmacol. Exp. Ther.* **291**, 531–537
5. Chase, T. N. (2004) *Parkinsonism Relat. Disord.* **10**, 305–313
6. Sucher, N. J., Awobuluyi, M., Choi, Y. B., and Lipton, S. A. (1996) *Trends Pharmacol. Sci.* **17**, 348–355
7. Standaert, D. G., Testa, C. M., Young, A. B., and Penney, J. B., Jr. (1994) *J. Comp. Neurol.* **343**, 1–16
8. Kosinski, C. M., Standaert, D. G., Counihan, T. J., Scherzer, C. R., Kerner, J. A., Daggett, L. P., Velicelebi, G., Penney, J. B., Young, A. B., and Landwehrmeyer, G. B. (1998) *J. Comp. Neurol.* **390**, 63–74
9. Yanahashi, S., Hashimoto, K., Hattori, K., Yuasa, S., and Iyo, M. (2004) *Brain Res.* **1011**, 84–93
10. Wang, Y. T., and Salter, M. W. (1994) *Nature* **369**, 233–235
11. Tingley, W. G., Ehlers, M. D., Kameyama, K., Doherty, C., Ptak, J. B., Riley, C. T., and Huganir, R. L. (1997) *J. Biol. Chem.* **272**, 5157–5166
12. Menegoz, M., Lau, L. F., Herve, D., Huganir, R. L., and Girault, J. A. (1995) *Neuroreport* **7**, 125–128
13. Oh, J. D., Russell, D. S., Vaughan, C. L., Chase, T. N., and Russell, D. (1998) *Brain Res.* **813**, 150–159

14. Salter, M. W., and Kalia, L. V. (2004) *Nat. Rev. Neurosci.* **5,** 317–328
15. Miyakawa, T., Yagi, T., Kitazawa, H., Yasuda, M., Kawai, N., Tsuboi, K., and Niki, H. (1997) *Science* **278,** 698–701
16. Yaka, R., Phamluong, K., and Ron, D. (2003) *J. Neurosci.* **23,** 3623–3632
17. Nakazawa, T., Komai, S., Tezuka, T., Hisatsune, C., Umemori, H., Semba, K., Mishina, M., Manabe, T., and Yamamoto, T. (2001) *J. Biol. Chem.* **276,** 693–699
18. Kojima, N., Ishibashi, H., Obata, K., and Kandel, E. R. (1998) *Learn. Mem.* **5,** 429–445
19. Cheung, H. H., and Gurd, J. W. (2001) *J. Neurochem.* **78,** 524–534
20. Yagi, T., Shigetani, Y., Okado, N., Tokunaga, T., Ikawa, Y., and Aizawa, S. (1993) *Oncogene* **8,** 3343–3351
21. Kulagowski, J. J., Broughton, H. B., Curtis, N. R., Mawer, I. M., Ridgill, M. P., Baker, R., Emms, F., Freedman, S. B., Marwood, R., Patel, S., Ragan, C. I., and Leeson, P. D. (1996) *J. Med. Chem.* **39,** 1941–1942
22. Watanabe, M., Fukaya, M., Sakimura, K., Manabe, T., Mishina, M., and Inoue, Y. (1998) *Eur. J. Neurosci.* **10,** 478–487
23. Yasunaga, M., Yagi, T., Hanzawa, N., Yasuda, M., Yamanashi, Y., Yamamoto, T., Aizawa, S., Miyauchi, Y., and Nishikawa, S. (1996) *J. Cell Biol.* **132,** 91–99
24. Boulay, D., Depoortere, R., Oblin, A., Sanger, D. J., Schoemaker, H., and Perrault, G. (2000) *Eur. J. Pharmacol.* **391,** 63–73
25. Lorenc-Koci, E., Wolfarth, S., and Ossowska, K. (1996) *Exp. Brain Res.* **109,** 268–276
26. Yuasa, S. (1996) *Anat. Embryol.* **194,** 223–234
27. Uchino, S., Watanabe, W., Nakamura, T., Shuto, S., Kazuta, Y., Matsuda, A., Nakajima-Iijima, S., Kudo, Y., Kohsaka, S., and Mishina, M. (2001) *FEBS Lett.* **506,** 117–122
28. Cepeda, C., Buchwald, N. A., and Levine, M. S. (1993) *Proc. Natl. Acad. Sci. U. S. A.* **90,** 9576–9580
29. Millan, M. J., Dekeyne, A., Rivet, J. M., Dubuffet, T., Lavielle, G., and Brocco, M. (2000) *J. Pharmacol. Exp. Ther.* **293,** 1063–1073
30. Miyakawa, T., Yagi, T., Kagiyama, A., and Niki, H. (1996) *Brain Res. Mol. Brain Res.* **37,** 145–150
31. Miyakawa, T., Yagi, T., Watanabe, S., and Niki, H. (1994) *Brain Res. Mol. Brain Res.* **27,** 179–182
32. Hironaka, N., Yagi, T., and Niki, H. (2002) *Brain Res. Mol. Brain Res.* **98,** 102–110
33. Xu, W., Doshi, A., Lei, M., Eck, M. J., and Harrison, S. C. (1999) *Mol. Cell* **3,** 629–638
34. Takasu, M. A., Dalva, M. B., Zigmond, R. E., and Greenberg, M. E. (2002) *Science* **295,** 491–495
35. de Souza, I. E., and Meredith, G. E. (1999) *Synapse* **32,** 243–253
36. Dragunow, M., Robertson, G. S., Faull, R. L., Robertson, H. A., and Jansen, K. (1990) *Neuroscience* **37,** 287–294
37. Ziolkowska, B., and Hollt, V. (1993) *Neurosci. Lett.* **156,** 39–42
38. Olney, J. W., and Farber, N. B. (1995) *Arch. Gen. Psychiatry* **52,** 998–1007
39. Tsai, G., and Coyle, J. T. (2002) *Annu. Rev. Pharmacol. Toxicol.* **42,** 165–179
40. Svensson, T. H. (2000) *Brain Res. Brain Res. Rev.* **31,** 320–329
41. Mohn, A. R., Gainetdinov, R. R., Caron, M. G., and Koller, B. H. (1999) *Cell* **98,** 427–436
42. Miller, A. L., Maas, J. W., Contreras, S., Seleshi, E., True, J. E., Bowden, C., and Castiglioni, J. (1993) *Biol. Psychiatry* **34,** 178–187
43. Chen, J. F., Moratalla, R., Impagnatiello, F., Grandy, D. K., Cuellar, B., Rubinstein, M., Beilstein, M. A., Hackett, E., Fink, J. S., Low, M. J., Ongini, E., and Schwarzschild, M. A. (2001) *Proc. Natl. Acad. Sci. U. S. A.* **98,** 1970–1975
44. Saga, Y., Kobayashi, M., Ohta, H., Murai, N., Nakai, N., Oshima, M., and Taketo, M. M. (1999) *Genes Cells* **4,** 219–228
45. Adams, M. R., Brandon, E. P., Chartoff, E. H., Idzerda, R. L., Dorsa, D. M., and McKnight, G. S. (1997) *Proc. Natl. Acad. Sci. U. S. A.* **94,** 12157–12161
46. Leveque, J. C., Macias, W., Rajadhyaksha, A., Carlson, R. R., Barczak, A., Kang, S., Li, X. M., Coyle, J. T., Huganir, R. L., Heckers, S., and Konradi, C. (2000) *J. Neurosci.* **20,** 4011–4020
47. Yaka, R., Thornton, C., Vagts, A. J., Phamluong, K., Bonci, A., and Ron, D. (2002) *Proc. Natl. Acad. Sci. U. S. A.* **99,** 5710–5715
48. Lu, W. Y., Xiong, Z. G., Lei, S., Orser, B. A., Dudek, E., Browning, M. D., and MacDonald, J. F. (1999) *Nat. Neurosci.* **2,** 331–338
49. Dwivedi, Y., and Pandey, G. N. (1999) *J. Pharmacol. Exp. Ther.* **291,** 688–704
50. Kotecha, S. A., Oak, J. N., Jackson, M. F., Perez, Y., Orser, B. A., Van Tol, H. H., and MacDonald, J. F. (2002) *Neuron* **35,** 1111–1122
51. Viviani, B., Bartesaghi, S., Gardoni, F., Vezzani, A., Behrens, M. M., Bartfai, T., Binaglia, M., Corsini, E., Di Luca, M., Galli, C. L., and Marinovich, M. (2003) *J. Neurosci.* **23,** 8692–8700

Journal of Neurochemistry, 2006, **97**, 1203–1214 doi:10.1111/j.1471-4159.2006.03831.x

Direct interaction of post-synaptic density-95/Dlg/ZO-1 domain-containing synaptic molecule Shank3 with GluR1 α-amino-3-hydroxy-5-methyl-4-isoxazole propionic acid receptor

Shigeo Uchino, Hidenori Wada, Shizuyo Honda, Yasuko Nakamura, Yumiko Ondo, Takayoshi Uchiyama, Moe Tsutsumi, Eri Suzuki, Takae Hirasawa and Shinichi Kohsaka

Department of Neurochemistry, National Institute of Neuroscience, Kodaira, Tokyo, Japan

Abstract

A class of scaffolding protein containing the post-synaptic density-95/Dlg/ZO-1 (PDZ) domain is thought to be involved in synaptic trafficking of α-amino-3-hydroxy-5-methyl-4-isoxazole propionic acid (AMPA) receptors during development. To clarify the molecular mechanism of AMPA receptor trafficking, we performed a yeast two-hybrid screening system using the cytoplasmic tail of the GluR1 subunit of AMPA receptor as a bait and identified a synaptic molecule, Shank3/ProSAP2, as a GluR1 subunit-interacting molecule. Shank3 is a PDZ domain-containing multidomain protein and is predominantly expressed in developing neurons. Using the glutathione S-transferase pull-down assay and immunoprecipitation technique we demonstrated that the GluR1 subunit directly binds to the PDZ domain of Shank3 via its carboxyl terminal PDZ-binding motif. We raised anti-Shank3 antibody to investigate the expression of Shank3 in cortical neurons. The pattern of Shank3 immunoreactivity was strikingly punctate, mainly observed in the spines, and closely matched the pattern of post-synaptic density-95 immunoreactivity, indicating that Shank3 is colocalized with post-synaptic density-95 in the same spines. When Shank3 and the GluR1 subunit were overexpressed in primary cortical neurons, they were also colocalized in the spines. Taken together with the biochemical interaction of Shank3 with the GluR1 subunit, these results suggest that Shank3 is an important molecule that interacts with GluR1 AMPA receptor at synaptic sites of developing neurons.

Keywords: α-amino-3-hydroxy-5-methyl-4-isoxazole propionic acid receptor, development, GluR1 subunit, post-synaptic density-95/ Dlg/ ZO-1 domain, Shank3, synapse.

J. Neurochem. (2006) **97**, 1203–1214.

Transmission at excitatory synapses is primarily mediated by glutamate acting on three classes of ligand-gated ion channels, α-amino-3-hydroxy-5-methyl-4-isoxazole propionic acid (AMPA), kainate and NMDA receptors (Wisden and Seeburg 1993; Hollmann and Heinemann 1994). In addition to their role in synaptic transmission, these glutamate receptors (GluRs) have been thought to play a crucial role in many brain functions, including activity-dependent synaptogenesis during development and synaptic plasticity (McDonald and Johnston 1990; Bliss and Collingridge 1993).

Many excitatory synapses in young developing neurons have been found to express only NMDA receptors, which are continuously blocked by magnesium at resting membrane potentials. As no evoked transmission is observed even when glutamate is present, these synapses are referred to as 'silent synapses'. During later development, AMPA receptors are delivered and clustered on the synaptic membrane in an activity-dependent manner, and the synapses subsequently become functionally active (Durand *et al.* 1996; Wu *et al.* 1996; Pickard *et al.* 2000; Liao *et al.* 2001; Isaac 2003). Thus, the clustering of AMPA receptors on the synaptic membrane is an essential event during synaptogenesis.

Received November 16, 2005; revised manuscript received February 2, 2006; accepted February 9, 2006.

Address correspondence and reprint requests to S. Kohsaka, Department of Neurochemistry, National Institute of Neuroscience, 4-1-1 Ogawahigashi, Kodaira, Tokyo 187-8502, Japan.
E-mail: kohsaka@ncnp.go.jp

Abbreviations used: aa, amino acid; AMPA, α-amino-3-hydroxy-5-methyl-4-isoxazole propionic acid; EGFP, enhanced green fluorescent protein; EGFP-GluR1, enhanced green fluorescent protein-fused GluR1 subunit; GluR, glutamate receptor; GST, glutathione S-transferase; mShank3, mouse Shank3; NR2B, NMDA receptor 2B; PBS, phosphate-buffered saline; PDZ, post-synaptic density-95/Dlg/ZO-1; PFA, paraformaldehyde; PSD-95, post-synaptic density-95; SAP-97, synapse-associated protein 97; SDS, sodium dodecyl sulfate; SH3, Src homology 3.

© 2006 The Authors
Journal Compilation © 2006 International Society for Neurochemistry,

The AMPA receptors are heteromeric complexes of four homologous subunits, GluR1–GluR4 (Wisden and Seeburg 1993; Hollmann and Heinemann 1994). The expression of GluR1–GluR3 subunits increases during development, whereas the expression of GluR4 subunit is seen in earlier development (Zhu *et al.* 2000). Recent studies have shown that induction of long-term potentiation or activation of Ca^{2+}/calmodulin-dependent protein kinase II promoted delivery of GluR1 subunit-containing AMPA receptors to synapses, and that this effect was diminished by mutating the post-synaptic density-95 (PSD-95)/Dlg/ZO-1 (PDZ) domain binding motif at the C-terminal end of the GluR1 subunit (Shi *et al.* 1999; Hayashi *et al.* 2000). This finding indicates that PDZ domain-containing proteins participate in regulating the synaptic localization of GluR1 subunit-containing AMPA receptors; however, this protein remains to be identified. So far, biochemical analysis has shown that GluR1 subunit binds to synapse-associated protein 97 (SAP-97) via its C-terminal PDZ-binding motif (Leonard *et al.* 1998). In developing neurons, however, expression of SAP-97 is distributed more in the somatic region than in the synapses. Thus, SAP-97 is thought to be associated with intracellular AMPA receptors, including GluR1 subunit, and to be involved in the early secretory pathway of AMPA receptor trafficking (Sans *et al.* 2001).

In this study, we used a yeast two-hybrid screening system to search for the protein that interacts with the PDZ-binding motif of GluR1 AMPA receptor, and we identified Shank3/ProSAP2 from the mouse brain cDNA library. Shank3 is a multidomain protein that contains ankyrin repeats, a Src homology 3 (SH3) domain, a PDZ domain, a long proline-rich region and a sterile alpha motif, and is predominantly expressed in spines during synaptogenesis (Lim *et al.* 1999; Naisbitt *et al.* 1999; Sheng and Kim 2000; Böckers *et al.* 2001, 2002). In the present study we found that Shank3 biochemically interacts with the PDZ-binding motif of GluR1 subunit and that Shank3 is colocalized with GluR1 AMPA receptor in the spines. These findings suggest that Shank3 is a candidate clue molecule for clarifying the molecular mechanism of AMPA receptor trafficking to synapses during synaptogenesis.

Materials and methods

Yeast two-hybrid screening

The cDNA fragment encoding the C-terminal 81-amino-acid segment [amino acids (aa) 809–889] of mouse GluR1 subunit was inserted into pLexA to yield a bait plasmid, pLexA-GluR1/C. The bait plasmid was transformed with yeast strain L40 and a mouse brain cDNA library (Clontech, Palo Alto, CA, USA) was used to screen for proteins that interacted with LexA-GluR1/C fusion proteins. Interactions were detected by induction of reporter genes, *HIS3*, *TRP1*, *LUE2* and *LacZ*, which resulted in cell growth and the formation of blue colonies on histidine-, tryptophan- and leucine-depleted yeast synthetic media containing X-gal (80 μg/mL).

Plasmid construction cDNA fragments encoding the full-length mouse Shank3 (mShank3; aa 1–1730), the SH3 and PDZ domains of mShank3 (mShank3/SH3-PDZ; aa 461–671), the PDZ domain (mShank3/PDZ; aa 552–671), the C-terminal fragment containing the PDZ domain (mShank3/PDZ + C; aa 552–1730) and the C-terminal fragment without the PDZ domain (mShank3/C; aa 670–1730) were constructed by PCR and subcloned into a mammalian expression vector, pCMV-Myc (Clontech), to obtain pCMV-myc-mShank3, pCMV-myc-mShank3/SH3-PDZ, pCMV-myc-mShank3/PDZ, pCMV-myc-mShank3/PDZ + C and pCMV-myc-mShank3/C, respectively. Fusion proteins of the regions of mShank3, GluR1 subunit and mouse NMDA receptor 2B (NR2B) (GluRε2) subunit with glutathione S-transferase (GST) (and myc) were constructed by subcloning PCR-amplified DNA fragments into pGEX-4T-2 (Amersham, Piscataway, NJ, USA) containing a thrombin cleavage site or into pGEX-5X-2 (Amersham) containing a factor Xa cleavage site to obtain: pGEX-4T-2, pGEX-mShank3/SH3-PDZ (aa 461–671), pGEX-mShank3/SH3 (aa 461–551), pGEX-mShank3/PDZ (aa 552–671), pGEX-myc-mShank3/SH3-PDZ (aa 461–671), pGEX-GluR1/C (aa 809–889), pGEX-GluR1/del (deletion of four aa from the C-terminal end) (aa 809–885), pGEX-GluR1/mu (exchange of four aa in the C-terminal end, ATGL to AAGA), pGEX-C-terminal segment of NR2B (aa 1279–1456), pGEX-5X-2 and pGEX-5X-GluR1/C (aa 809–889). All of the constructs were confirmed by DNA sequencing.

Cell culture and DNA transfection

Chinese hamster ovary cells or COS7 cells were grown at 37°C in a humidified 5% CO_2 atmosphere in Dulbecco's modified Eagle's medium (Gibco BRL, Grand Island, NY, USA) containing 10% heat-inactivated fetal bovine serum (Irvine, Santa Ana, CA, USA). For the transient expression studies, the cells were transfected with expression vector by using Lipofectamine Plus (Invitrogen, Carlsbad, CA, USA) according to the manufacturer's protocol.

Embryonic day 15–16 mouse cortical primary neurons were prepared as described previously (Hirasawa *et al.* 2003). Briefly, cerebral cortices were dissected, minced and dissociated with a papain. The dissociated cells were plated onto 0.1% polyethylenimine-coated plates at a density of $1.0–1.5 \times 10^4$ cells/cm^2 for immunocytochemistry and 1.0×10^5 cells/cm^2 for pull-down assays, and maintained in Neurobasal medium (Gibco BRL) containing 2% B-27 supplement (Gibco BRL) and 0.5 mM glutamine at 37°C under a humidified 10% CO_2 atmosphere for the periods indicated. For the transient expression studies, the cells were transfected with expression vector by using Lipofectamine 2000 (Invitrogen) according to the manufacturer's protocol.

The experimental protocols were approved by The Animal Care and Use Committee of the National Institute of Neuroscience.

Purification of recombinant proteins and pull-down assay

The GST fusion proteins were expressed in *Escherichia coli* BL21 and purified on glutathione sepharose 4B (Amersham) according to the manufacturer's protocol. The pull-down assay was performed essentially as described previously (Tu *et al.* 1999). Briefly, the Chinese hamster ovary cells transfected with myc-tagged protein or mouse cortical primary cells were lysed at 4°C for 1 h with a buffer

© 2006 The Authors

composed of 50 mM Tris-HCl (pH 7.5), 100 mM NaCl, 1 mM EDTA, protease inhibitor cocktail (Roche, Penzberg, Germany) and 0.1% Triton X-100 (for Chinese hamster ovary cells) or 1% Triton X-100 (for primary cultured cells). After removing the insoluble material by centrifugation (15 000 *g* for 20 min at 4°C), the protein concentration in the supernatant was determined with a protein assay kit (Pierce, Rockford, IL, USA). Soluble extracts were incubated for 12 h at 4°C with purified GST fusion protein bound to 20 μL of glutathione sepharose in phosphate-buffered saline (PBS) containing 0.1% Triton X-100 and protease inhibitor cocktail. The sepharose suspensions were washed four times with lysis buffer. Bound proteins were eluted by boiling in sodium dodecyl sulfate (SDS) sample buffer, separated by SDS–polyacrylamide gel electrophoresis and analysed by immunoblot.

Immunoprecipitation assay

COS7 cells were transfected with each of the expression vectors. At 2 days after transfection, cells were lysed at 4°C for 1 h with immunoprecipitation (IP) buffer composed of 50 mM Tris-HCl (pH 7.5), 150 mM NaCl, 0.5 mM EDTA, 10% glycerol, 0.5% Triton X-100 and protease inhibitor cocktail. After removing the insoluble material by centrifugation (15 000 *g* for 20 min at 4°C), the protein concentration in the supernatant was determined with a protein assay kit. Soluble extracts were incubated at 4°C for 2 h with rabbit polyclonal anti-enhanced green fluorescent protein (EGFP) antibody bound to protein A- and G-Sepharose beads (Amersham). The immunoprecipitates were washed three times with IP buffer, eluted by boiling in SDS sample buffer, separated by SDS–polyacrylamide gel electrophoresis and analysed by immunoblot.

Antibody production

Rabbit polyclonal antibody against a GST-fused mShank3 fragment (aa 1016–1357) was produced by Biotest Inc. (Tokyo, Japan).

Preparation of the synaptosomal fraction

The synaptosomal fraction was prepared essentially according to the procedures described previously (Carlin *et al.* 1980). In brief, cortex was dissected from mouse at 2 weeks of age and homogenized in 10 volumes of solution A (0.32 M sucrose, 1 mM $NaHCO_3$, 1 mM $MgCl_2$ and 0.5 M $CaCl_2$) with a Teflon homogenizer. The homogenate was centrifuged (1400 *g* for 10 min at 4°C) and the supernatant was saved. The pellet was suspended in solution A and centrifuged (700 *g* for 10 min at 4°C). The supernatants were pooled and then centrifuged (13 800 *g* for 10 min at 4°C). The resulting pellet was resuspended in solution B (0.32 M sucrose and 1 mM $NaHCO_3$), layered onto a discontinuous sucrose gradient containing 0.8 M/1.0 M/1.2 M sucrose and centrifuged (82 500 *g* for 2 h at 4°C). The fraction at the 1.0 M/1.2 M sucrose interface was isolated as the synaptosomal fraction and the protein concentration was determined with a protein assay kit.

Immunoblot analysis

The proteins were separated by electrophoresis through an SDS polyacrylamide gel (Daiichi Pure Chemicals, Tokyo, Japan) and then electrophoretically transferred to nitrocellulose membranes (Schleicher & Schuell, Dassel, Germany). The membranes were blocked by incubation for 1 h at room temperature (15~25°C) with 5% skim milk (Becton Dickinson, Sparks, MD, USA) in buffer A (10 mM Tris-HCl, pH 7.5, 100 mM NaCl and 0.1% Tween 20) and then incubated for 1 h at room temperature with one of the following primary antibodies in buffer A containing 3% skim milk: rabbit polyclonal anti-mShank3 antibody (0.1 μg/mL), mouse monoclonal anti-myc antibody (1 : 1000; Roche), mouse monoclonal anti-PSD-95 antibody (1 : 200; Affinity Bioreagents Inc., Golden, CO, USA), rabbit polyclonal anti-GluR1 antibody (1 : 200; Chemicon, Temecula, CA, USA), rabbit polyclonal anti-GluR2 antibody (1 : 200; Chemicon) or rabbit polyclonal anti-EGFP antibody (1 : 1000; Molecular Probes, Eugene, OR, USA). After three washes in buffer A, the membranes were incubated for 1 h at room temperature with horseradish peroxidase-conjugated anti-rabbit IgG secondary antibody (1 : 1000; Amersham) or horseradish peroxidase-conjugated anti-mouse IgG secondary antibody (1 : 1000; Amersham) and washed three times with buffer A. Immunoreactive bands were visualized with a chemiluminescence detection system (ECL; Amersham).

Preparation of membrane fraction and coimmunoprecipitation assay

To prepare the membrane fraction, the cortex was dissected from mouse at 2 weeks of age and homogenized with a Teflon homogenizer in PBS containing 0.25 M sucrose and protease inhibitor cocktail. The homogenate was centrifuged at 2000 *g* for 10 min to remove nuclei and debris, at 8000 *g* for 30 min to remove mitochondria and then at 100 000 *g* for 1 h to obtain the pellet as membrane fraction. The membrane proteins were solubilized at 4°C for 2 h with 2% SDS in PBS containing protease inhibitor cocktail and then diluted with five volumes of 2% Triton-X-100 in PBS as described in the previous study in which the binding of Kir 2.3 and PSD-95 was confirmed (Cohen *et al.* 1996). They were subsequently incubated at 4°C for 2 h with rabbit polyclonal anti-Shank3 antibody bound to protein A- and G-Sepharose beads. The immunoprecipitates were washed three times with IP buffer composed of 50 mM Tris-HCl (pH 7.5), 150 mM NaCl, 0.5 mM EDTA, 10% glycerol, 0.5% Triton X-100 and protease inhibitor cocktail, eluted by boiling in SDS sample buffer, separated by SDS–polyacrylamide gel electrophoresis and analysed by immunoblot.

Immunocytochemistry

Primary cells were fixed with 2% paraformaldehyde (PFA) for 10 min at room temperature. After three washes in PBS, the cells were permeabilized and blocked with 3% goat serum/0.1% Triton X-100 in PBS for 15 min, and then incubated for 1 h at room temperature with one of the following primary antibodies in PBS containing 3% bovine serum albumin (Sigma, St Louis, MO, USA): rabbit polyclonal anti-mShank3 antibody (1.0 μg/mL), mouse monoclonal anti-PSD-95 antibody (1 : 200), mouse monoclonal anti-myc antibody (1 : 500) or rabbit polyclonal anti-EGFP antibody (1 : 500). After three washes in PBS, the cells were incubated for 1 h at room temperature with Alexa Fluor 488 goat anti-mouse IgG (H + L) (1 : 1000; Molecular Probes), Alexa Fluor 488 goat anti-rabbit IgG (H + L) (1 : 1000; Molecular Probes), Alexa Fluor 594 goat anti-mouse IgG (H + L) (1 : 1000; Molecular Probes) or Alexa Fluor 594 goat anti-rabbit IgG (H + L) (1 : 1000; Molecular Probes) in PBS containing 3% bovine serum albumin. After three washes in PBS, the cells were mounted on a glass slide with PermaFluor (Thermo Shandon, Pittsburgh, PA, USA) containing

© 2006 The Authors

10% FluoroGuard (Bio-Rad, Hercules, CA, USA) to inhibit photobleaching and examined with a fluorescence microscope (AX70; Olympus, Tokyo, Japan). For surface staining of EGFP-fused GluR1 subunit (EGFP-GluR1), cells were first incubated for 20 min at room temperature with rabbit polyclonal anti-EGFP antibody (1 : 500) in PBS and, after washing in PBS, they were incubated for 20 min at room temperature with Alexa Fluor 488 goat anti-rabbit IgG (H + L) (1 : 1000) in PBS and fixed with 2% PFA for 10 min. They were then permeabilized and blocked for 15 min with 3% goat serum/0.1% Triton X-100 in PBS for subsequent immunostaining.

In situ hybridization

Three cDNA fragments (620 bp, 650 bp and 1 kb) of the unique region of mShank1, mShank2 and mShank3, respectively, were obtained by PCR and subcloned into mammalian expression vector pCMV-SPORT (Gibco BRL). Sense and antisense digoxigenin-labeled probes were produced with SP6 and T7 polymerase, respectively.

Brain specimens were prepared from mice as follows. Anesthetized mice were transcardially perfused with 4% PFA in PBS. Their brains were removed from the skulls and immersed in 4% PFA at 4°C for 2 days, and then in 30% sucrose at 4°C for 2 days. After embedding in optimal cutting temperature compound (Sakura Finetechnical Co. Ltd, Tokyo, Japan), they were quickly frozen in dry ice. Frozen brain sections (14 μm thick) were cut in the sagittal plane with a cryostat (CM-3000; Leica, Nussloch, Germany) and the sections were mounted on 3-aminopropyltriethoxysilane-coated glass slides (Matsunami, Osaka, Japan) and stored at – 80°C until use.

For hybridization, the sections were treated with 4 μg/mL pepsin/0.2 N HCl for 2 min at 37°C, washed twice in PBS containing 0.1% Tween 20 and post-fixed with 4% PFA for 30 min. After washing in PBS containing 0.1% Tween 20 for 5 min, the sections were treated with 0.2% diethylpyrocarbonate in PBS containing 0.1% Tween 20 and hybridized at 65°C for 16 h with 10 μg/mL digoxigenin-labeled probe in a buffer composed of 50% formamide, 5× saline sodium citrate, 1% SDS, 50 μg/mL heparin and 50 μg/mL yeast RNA. They were then washed for 30 min at 65°C in 5× saline sodium citrate containing 50% formamide and 1% SDS, and then twice for 45 min at 65°C in 2× saline sodium citrate containing 50% formamide. After washing in TBS-T (136 mM NaCl, 2.7 mM KCl, 250 mM Tris-HCl, pH 7.5, 0.1% Tween 20) for 20 min at room temperature, they were blocked with 0.2% blocking reagent (Roche) for 40 min and incubated with alkaline phosphatase-conjugated anti-digoxigenin Fab fragments (1 : 2000; Roche) diluted in blocking solution at 4°C for 16 h. They were then washed in TBS-T for 20 min at room temperature and alkaline phosphatase-conjugated antibody was visualized by reaction with 35 μg/mL 4-nitroblue tetrazolium chloride/17.5 μg/mL 5-bromo-4-chloro-3-indolyl-phosphate (Roche) in 100 mM Tris-HCl (pH 9.5), 100 mM NaCl, 50 mM $MgCl_2$, 0.1% Tween 20 and 2 mM levamisole (Sigma) at room temperature for 1–2 nights in the dark. The color reaction was stopped with deionized water and the sections were dehydrated in a graded ethanol series and mounted with Entellan (Merck, Darmstadt, Germany).

RT-PCR

Total RNA was extracted from mouse cortex with acid guanidinium thiocyanate-phenol-chloroform (Chomczynski and Sacchi 1987) and RT-PCR was performed by using an Advantage RT for PCR kit (Clontech) according to the manufacturer's protocol. The thermocycle profile for PCR amplification was: 30 s at 95°C, 30 s at 55°C, 1 min at 72°C for 30 cycles (mShank1), 33 cycles (mShank2 and mShank3) or 22 cycles (glyceraldehyde-3-phosphate dehydrogenase used as an internal control). The PCR products were separated on a 3% agarose gel and stained with ethidium bromide. The gel images were fed into an image processor (Archiver Eclipse; Fotodyne, Hartland, WI, USA) and quantitatively analysed with NIH imaging software. The primers for PCR analysis were: for mShank1, forward GGCAGGCGTAG-GAAGCTCTA and reverse CTCATCCATGTCTGGGTG; for mShank2, forward TATGATGAGCGTCCCCGGCGG and reverse ATCATCAGGGTCTAGATT; for mShank3, forward GGCCC-GAAGCGGAAACTTT and reverse ACCATCCTCCTCGGGTTT; and for glyceraldehyde-3-phosphate dehydrogenase, forward GTCATCATCTCCGCCCCTTCTGC and reverse GATGCCTGC-TTCACCACCTTCTTG.

Results

Screening for proteins that interact with GluR1 subunit of α-amino-3-hydroxy-5-methyl-4-isoxazole propionic acid receptor

We used a yeast two-hybrid method to identify proteins that interact with GluR1 subunit of AMPA receptor. Using the C-terminal 81-amino-acid segment of GluR1 subunit as yeast two-hybrid bait, we identified several clones from among approximately 1×10^7 mouse brain clones. Sequencing analysis revealed that one of them, clone 321, encoded the C-terminal 1305-amino-acid segment of Shank3, which includes the SH3 and PDZ domains (Fig. 1a). We then cloned full-length Shank3 cDNA from mouse brain by RT-PCR. The deduced mShank3 protein showed 98% sequence identity with rat Shank3.

Shank3 is a multidomain protein that contains ankyrin repeats, an SH3 domain, a PDZ domain, a long proline-rich region and a sterile alpha motif (Fig. 1a), and it scaffolds various proteins, including guanylate kinase-associated protein (GKAP) and Homer, in excitatory post-synapses (Naisbitt *et al.* 1999; Sheng and Kim 2000; Böckers *et al.* 2001). We initially focused on the SH3 and PDZ domains of mShank3, as they are important for interaction with proteins. We investigated the biochemical interaction between mShank3 and GluR1 subunit by GST pull-down assay using the GST-fused SH3 and PDZ domains of mShank3 (GST-mShank3/SH3-PDZ) and extracts from mouse cortical primary cells. GST-mShank3/SH3-PDZ clearly pulled down GluR1 subunit, indicating that mShank3 binds to GluR1 subunit through the SH3-PDZ domains (Fig. 1b). In addition, we examined the other synaptic molecules, GluR2 subunit of AMPA receptor and PSD-95. As shown in Fig. 1(b), GST-mShank3/SH3-PDZ pulled down PSD-95 but not GluR2 subunit.

© 2006 The Authors
Journal Compilation © 2006 International Society for Neurochemistry,

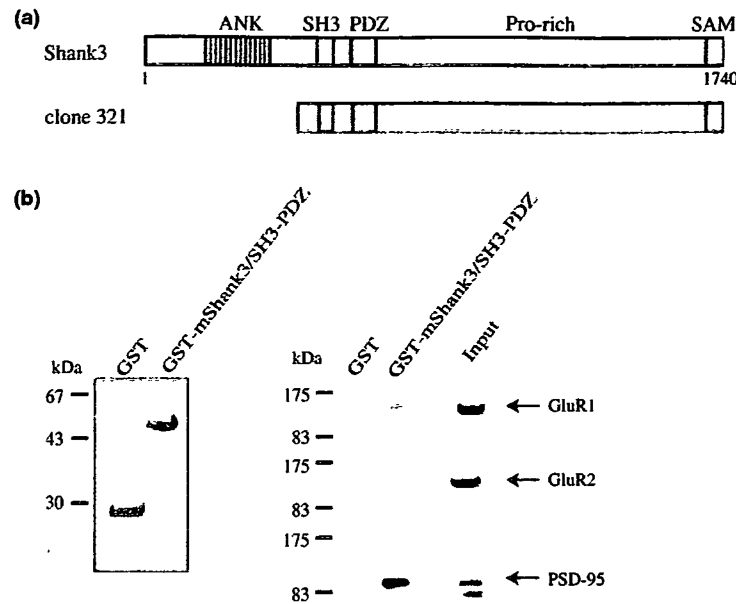

Fig. 1 Schematic structure of Shank3 and the biochemical interaction of mouse Shank3 (mShank3) with GluR1 subunit. (a) The schematic structure of Shank3 and clone 321. ANK, Ankyrin repeats 1–7; SH3, Src homology 3 domain; PDZ, post-synaptic density-95/Dlg/ZO-1 domain; SAM, sterile alpha motif. (b) Pull-down assay. The left panel shows the purified glutathione S-transferase (GST) and GST-fused mShank3/SH3-PDZ separated by sodium dodecyl sulfate–polyacrylamide gel electrophoresis (SDS–PAGE), and the right panel shows the immunoblots. GST alone or GST-fused mShank3/SH3-PDZ bound to glutathione sepharose beads was incubated with 1 mg of extract from mouse cortical primary cells cultured for 14 days. After washing, the proteins on the beads were eluted with SDS–PAGE sample buffer and immunoblotted with anti-GluR1 antibody, anti-GluR2 antibody or anti-post-synaptic density-95 (PSD-95) antibody. The input lane was loaded with 25 μg of the primary cell extract. Molecular weight standards are shown on the left.

Post-synaptic density-95/Dlg/ZO-1 domain of mouse Shank3 directly binds to the C-terminal segment of GluR1 subunit

To identify the interactive domain of mShank3, we constructed GST-mShank3/SH3, GST-mShank3/PDZ and GST-mShank3/SH3-PDZ (Fig. 2a), and performed a GST pull-down assay using cell lysates of Chinese hamster ovary cells expressing the myc-tagged C-terminal 81-amino-acid segment of GluR1 (myc-GluR1/C). As shown by SDS–polyacrylamide gel electrophoresis (Fig. 2a), the concentrations of each of the purified GST fusion proteins were almost the same. GST-mShank3/SH3-PDZ and GST-mShank3/PDZ clearly pulled down myc-GluR1/C, whereas no binding of GST-mShank3/SH3 to myc-GluR1/C was detected (Fig. 2a). These results suggest that GluR1 interacts with mShank3 via the PDZ domain.

We next investigated whether the interaction between mShank3/SH3-PDZ and GluR1/C was direct. The GST-fused myc-tagged SH3-PDZ domain of mShank3 (GST-myc-mShank3/SH3-PDZ) was expressed in *E. coli* BL21. After purification with glutathione sepharose, thrombin was reacted at 37°C for 1 h with the GST-myc-mShank3/SH3-PDZ bound to glutathione sepharose beads in PBS and purified myc-tagged mShank3/SH3-PDZ was obtained. GST-GluR1/C was produced using pGEX-5X-2 vector to protect against thrombin digestion and pull-down assays were performed. As shown in Fig. 2(b), purified myc-mShank3/SH3-PDZ bound to GST-GluR1/C, indicating that mShank3/SH3-PDZ binds directly to GluR1/C.

GluR1 subunit binds to the post-synaptic density-95/Dlg/ZO-1 domain of mouse Shank3 through its C-terminal post-synaptic density-95/Dlg/ZO-1 binding motif

As the C-terminal sequence of GluR1 subunit, -ATGL, is a typical PDZ-binding motif, -X-T/S-X-V/L/I (X represents any aa) (Songyang *et al.* 1997), we investigated whether the interaction between the PDZ domain of mShank3 and GluR1 subunit is mediated by the PDZ-binding motif of GluR1 subunit. To precisely identify the C-terminal residues involved in the binding, we prepared mutated GluR1/C carrying AAGA residues instead of ATGL and deleted GluR1/C lacking ATGL residues at its C-terminal end (Fig. 3a), and binding of these GluR1/C mutants to myc-mShank3/SH3-PDZ was almost abolished (Fig. 3b). The NR2B subunit, which binds to the PDZ domain of PSD-95, also has a PDZ-binding motif at its C-terminal end, -ESDV; however, the C-terminal segment of NR2B did not bind to myc-mShank3/SH3-PDZ (Fig. 3b). These findings demonstrate that the final four aa of GluR1 subunit are important for specific binding to the PDZ domain of mShank3.

© 2006 The Authors
Journal Compilation © 2006 International Society for Neurochemistry,

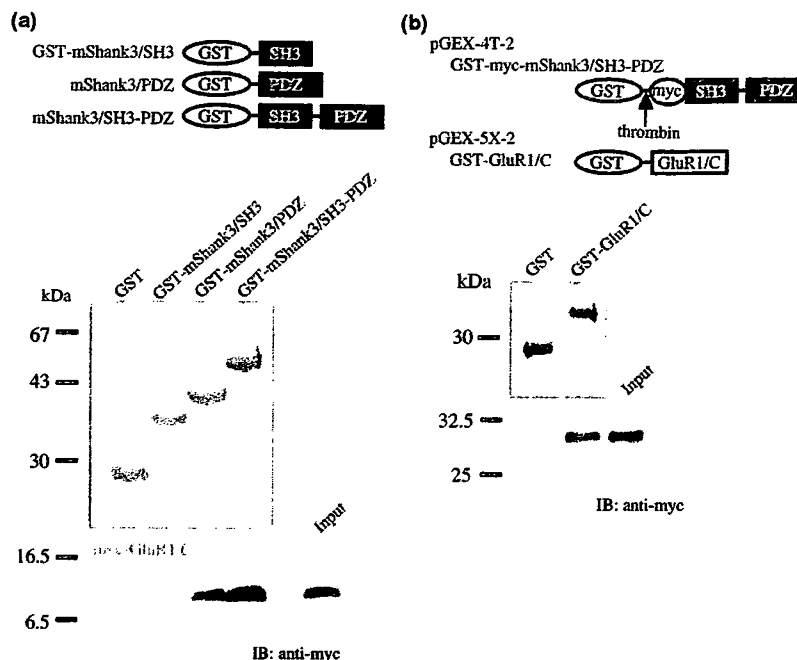

Fig. 2 Direct interaction of mouse Shank3 (mShank3) with GluR1 subunit. (a) Pull-down assay. The schematic structure of glutathione S-transferase (GST)-fused mShank3 mutants is shown at the top. The upper panel shows the purified GST and GST-fused mShank3 proteins separated by sodium dodecyl sulfate–polyacrylamide gel electrophoresis (SDS–PAGE) and the lower panels show the immunoblot. GST alone or each of the GST-fusion proteins bound to glutathione sepharose beads was incubated with 400 μg of extract from Chinese hamster ovary (CHO) cells transfected with myc-tagged GluR1/C. After washing, the proteins on the beads were eluted with SDS–PAGE sample buffer and immunoblotted with anti-myc antibody. The input lane was loaded with 30 μg of the CHO cells extract. (b) Pull-down assay. The schematic structure of GST-fused mShank3/SH3-PDZ and GluR1/C is shown at the top. The upper panel shows the purified GST and GST-fused GluR1/C proteins separated by SDS–PAGE and the lower panels show the immunoblots. GST alone or GST-fused GluR1/C bound to glutathione sepharose beads was incubated with purified myc-Shank3/SH3-PDZ. After washing, the proteins on the beads were eluted with SDS–PAGE sample buffer and immunoblotted with anti-myc antibody. The input lane was loaded with 5% of the purified myc-Shank/SH3-PDZ used for the pull-down assay. Molecular weight standards are shown on the left. PDZ, post-synaptic density-95/Dlg/ZO-1; SH3, Src homology 3; IB, immunoblot.

We then investigated the interaction between mShank3 and full-length GluR1 subunit by immunoprecipitation experiments. We constructed myc-tagged mShank3 (myc-mShank3) and the four deletion mutants as shown in Fig. 4(a), and expressed them together with EGFP-GluR1 in COS7 cells. Anti-EGFP antibody coimmunoprecipitated myc-mShank3, myc-mShank3/PDZ + C, myc-mShank3/SH3-PDZ and myc-mShank3/PDZ from cell lysates of COS7 cells expressing EGFP-GluR1 and myc-mShank3 or deletion mutants but not myc-mShank3/C (Fig. 4b). No signals were observed with immunoprecipitates obtained with normal IgG. These results indicate that the PDZ domain of mShank3 is indispensable to the interaction with GluR1 subunit.

Mouse Shank3 is expressed in the spine of the cortical neurons and interacts with GluR1 α-amino-3-hydroxy-5-methyl-4-isoxazole propionic acid receptor

To study native mShank3 protein, rabbit polyclonal antibodies were raised against the GST-fused 342-aa segment of mShank3 (aa 1016–1357). To confirm the specificity of the anti-mShank3 antibody, we transiently transfected COS cells with myc-mShank3 to allow the use of anti-myc antibody as a positive control. As shown in Fig. 5(a), the immunoreactive band for anti-mShank3 antibody (240 kDa) was identical to that for anti-myc antibody and no bands were detected in the COS7 cells transfected with myc vector, indicating that the anti-mShank3 antibody specifically detected mShank3 protein. mShank3-immunoreactive bands were observed in mouse cortical lysates and disappeared upon coincubation with antigen GST-fused mShank3 segment but not with GST alone (data not shown). We also confirmed the presence of mShank3 in the synaptosomal fraction as well as GluR1 subunit and PSD-95 (Fig. 5b).

To verify the interaction between mShank3 and GluR1 AMPA receptor *in vivo*, we performed a coimmunoprecipitation assay with membrane fraction prepared from mouse cortex using anti-Shank3 antibody (Fig. 5c). Shank3 antibody efficiently immunoprecipitated endogenous mShank3

© 2006 The Authors